UNIVERSITA' POLITECNICA DELLE MARCHE

Department of Industrial Engineering and Mathematical Sciences

Faculty of Engineering

Master's Degree in Biomedical Engineering

Characterization of a respiratory triggered nebulizer for surfactant drug delivery in newborns

Thesis Advisor:

Prof. Lorenzo Scalise

Thesis Supervisor:

Luca Antognoli

Candidate:

Rosamaria Terzano

Academic Year **2022** / **2023**

Abstract

The respiratory system has an essential role in the life of an individual, and it is therefore necessary for his condition to be optimal. This system begins to develop from the first weeks of pregnancy and then gradually completes until the last periods of gestation. However, there are cases of premature births, due to several factors, that involve the birth of newborns before the full maturity of the respiratory system, with more or less severe conditions depending on the degree of prematurity. This condition of immaturity of the respiratory system can lead to a condition in which a substance of fundamental importance for respiratory functions is not enough: the surfactant. The latter has surfactant properties and creates, at the level of the alveoli, thin films that combat surface pressure to prevent alveoli from collapse. A lack of surfactant leads to breathing difficulties that can be fatal, and generally, such a condition requires the need for mechanical ventilation to help the subject in respiratory functions. Assisted ventilation is supported by surfactant replacement therapy, in which exogenous surfactant administration is performed. This is usually done by endotracheal procedure, but since it is an invasive and risky technique, nebulization is a good alternative. There are several nebulization devices, and in particular, this study focuses on the analysis of the particles produced by a pulmonary surfactant nebulizer, in relation to several other nebulization devices. Precisely, the study aims to conduct a comprehensive evaluation of the nebulizer's performance, in terms of particle velocity and size distributions, evaluated according to the change of two test parameters: the pressure of compressed air and the blowing time. A special measurement setup has been created to carry out the acquisitions with the nebulizer, which are studied through an algorithm generated to automate the acquisition of particle velocity and diameter. The analysis showed that a good combination of parameters is a pressure of 3 bar and a blowing time of 0.3 s. However, although the combination is the best among those

considered, the result is not yet optimal to consider the system suitable for spraying surfactant for therapy, since the particles produced are too large and slow. There are particles with an average speed of 0.39 m/s and a diameter of about 0.3 mm, still too large to reach the lower airways, therefore the alveoli, for which a diameter of 1-5 μm is necessary.

Index

Introduction 1

Chapter 1: State of the art 3

1.1. Respiratory system 3

1.2. Surfactant 10

1.3. Respiratory Distress Syndrome 13

1.4. Nebulization system 19

Chapter 2: Materials and Methods 24

2.1. Measurement setup 24

2.2. Acquisition and test parameters 32

2.3. Measurement protocol 34

2.4. Calibration 36

2.5. Data analysis 38

2.5.1. Creation of the tracker 38

2.5.2. Velocity and dimension distribution 44

Chapter 3: Results 50

Chapter 4: Discussion and Conclusion 65

4.1. Discussion and conclusion 65

4.2. Suggestion for future studies 69

Figure index 71

Table index 74

Bibliography 75

Introduction

The development of an individual's respiratory system begins around the sixth week of gestation, ending around the thirty-sixth. A good level of maturation of the respiratory system, though not complete, is reached after about 25 weeks of pregnancy, when the alveoli and in particular type II pneumocytes begin to produce a substance known as surfactant. The surfactant is a substance with surfactant properties, which ensures the proper functioning of the respiratory mechanism. It helps in the correct alternation of inhalation and exhalation phases, affecting the surface tension. In particular, the surfactant is composed of amphipathic molecules, therefore characterized by both a hydrophobic and hydrophilic component, which create thin films on the surface of the alveoli, reducing surface tension and preventing alveolar collapse during the exhalation phase. In case of premature birth, the newborn may not have sufficient surfactant to ensure the correct lung mechanism, leading to respiratory distress syndrome (RDS). To reduce the impact of RDS on the newborn's development, it is convenient to intervene with the exogenous administration of surfactant, possible through different types of techniques, in conjunction with mechanical ventilation. Generally, the administration of surfactant is by bolus, but a valid alternative for the reduction of damage is nebulization. The objective of this study is to analyze a pulmonary nebulization system intended for premature infants suffering from respiratory disorders. In particular, the study focuses on the development of an algorithm capable of capturing video of surfactant nebulisations and, from these, analyzing the properties of nebulized particles. The algorithm analyzes the velocity and diameter of the particles, going to consider different combinations of test parameters, namely pressure and blowing time. The study focuses on developing an algorithm that captures video of surfactant nebulizations and analyzes the properties of

nebulized particles, including their velocity and diameter. The algorithm considers different combinations of test parameters, namely pressure and blowing time, to identify the best configuration of parameters and assess whether the device is efficient for surfactant replacement therapy.

Chapter 1: State of the art

1.1. Respiratory system

The respiratory system encompasses all the organs and structures that allow gaseous exchanges between the environment, from which oxygen is obtained, and the body, which is rich in carbon dioxide. In the respiratory system, two large sections can be highlighted: the first, in particular, is responsible for the conduction and circulation of air, and the second, which represents the bottom of the structure, is in charge of gaseous exchanges. It consists of the nose, pharynx, larynx, trachea, lungs, pleura, bronchi, and bronchioles. The nose is the initial part of the respiratory tract, consisting of two nasal passages, mucous-lined canals that at the end create the nostrils. The pharynx is a canal that connects the throat and esophagus, and it forms both the first part of the digestive tract and part of the respiratory tract, as air inhaled through the nose reaches it, which then reaches the larynx. The latter allows the passage of inhaled air from the nose into the bronchi and vice versa. The connection between the larynx and the bronchi is ensured by the presence of the trachea, which branches into two sections to generate the two bronchial trees. The bronchi are conduits that facilitate the passage of air first to the bronchioles and then to the alveoli. The bronchioles are the small final branches of the bronchi inside the lungs and branch several times until they reach the alveoli at their ends. A representation of the respiratory system is shown in Figure 1 (Fig.1).

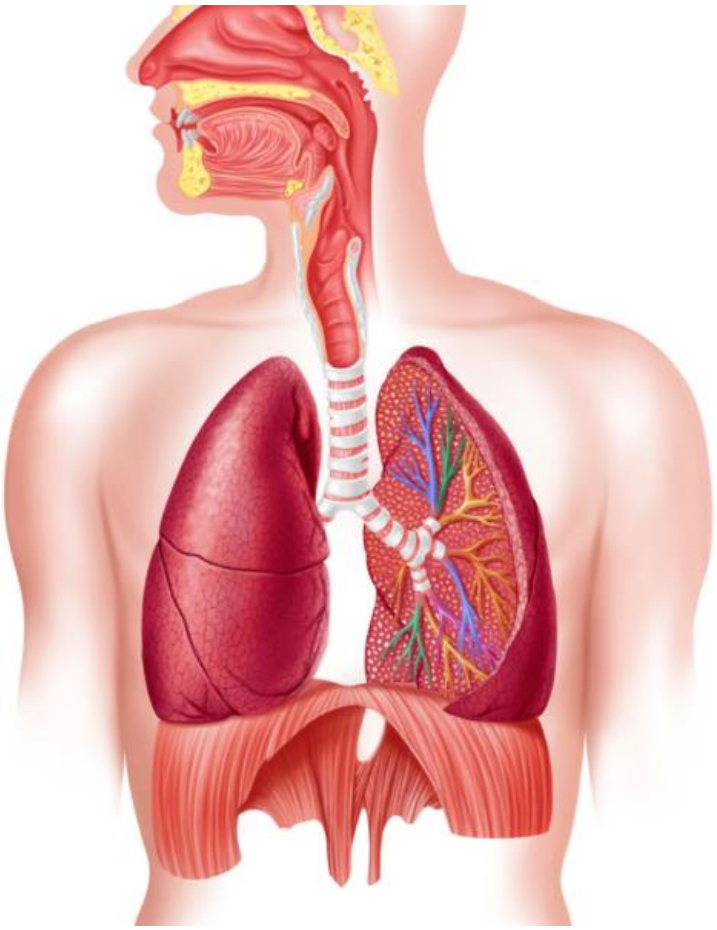

Fig. 1: Respiratory system

The alveolus represents the functional unit of the lung; in fact, more than 400 million can be found within the two lungs [1]. They are organised in a grape-like structure that forms the final part of the airways and through whose walls gas exchanges with the blood take place (Fig.2).

The respiratory system is responsible for ventilation, ensured by the cyclic process of inspiration exhalation, and is also responsible for the gaseous exchange of oxygen and carbon dioxide between the atmosphere and the bloodstream at the level of the alveoli. This exchange of respiratory gases occurs through a relatively complex physical barrier, consisting of the thin aqueous film that lines the alveolus, the alveolar epithelial cells, the interstitial layer, the

endothelial cells that form the blood capillaries, the blood plasma, and, finally, the erythrocyte membrane. Due to the fluid coating inside the alveoli, which is a consequence of cell metabolism, the lungs must cope with surface tension at the interface between the hypophasic fluid and air [2].

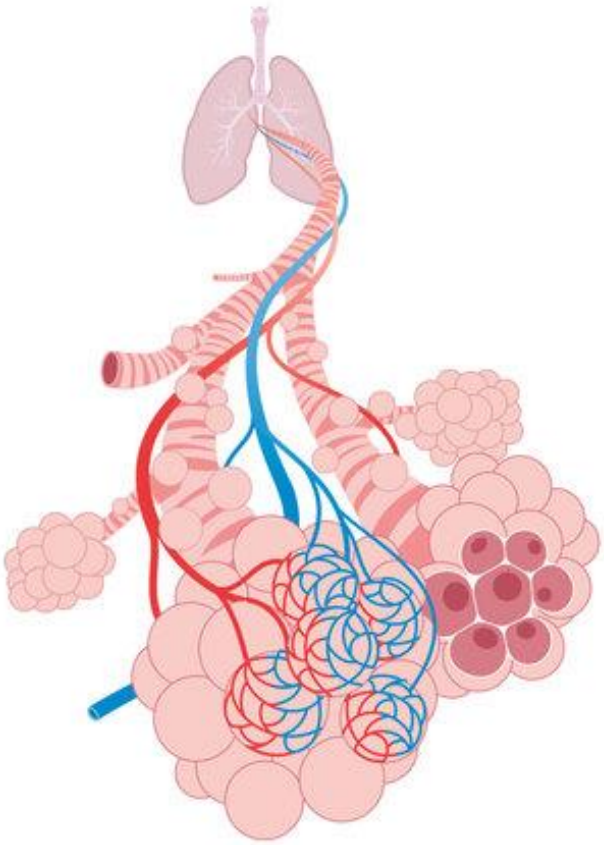

Fig. 2: Representation of pulmonary alveoli.

Each alveolus consists of a thin epithelial layer that lines a small cavity, which, in addition to a thin layer of water, contains a surface-active substance known as surfactant.

From a global point of view, the lower section of the respiratory apparatus allows the exchange of oxygen and carbon dioxide between the inside of the body and the outside

environment, through an anatomical connection with a thin structure known as the alveolocapillary barrier, a few μm thick [1]. The alveoli and the last branches of the bronchi are located inside the lungs, organs involved in respiration, with the main task of transporting oxygen to the organism and expelling carbon dioxide through processes of gaseous exchange between the environment and the blood, known as the processes of haematosis. Specifically, the lungs receive carbon dioxide-rich blood to eliminate it and make the blood oxygenated, and then send it to the heart and allow it to propagate from it to the rest of the body. Each lung is enveloped by a membrane, consisting of two layers, called pleural leaflets, and known as the pleura. The parietal pleura covers the surface of the lung and insulates it from the environment of the ribcage; the visceral pleura lines the inner wall of the lung. The pleura's main role is to facilitate the breathing mechanism, allowing the lungs to slide over the walls of the lung cavity during the inhalation and exhalation phases [3]. Specifically, in the space between the two pleural leaflets, there is a negative pressure, which allows the lungs to expand during the inhalation phase and receive air from the external environment Fig 3.

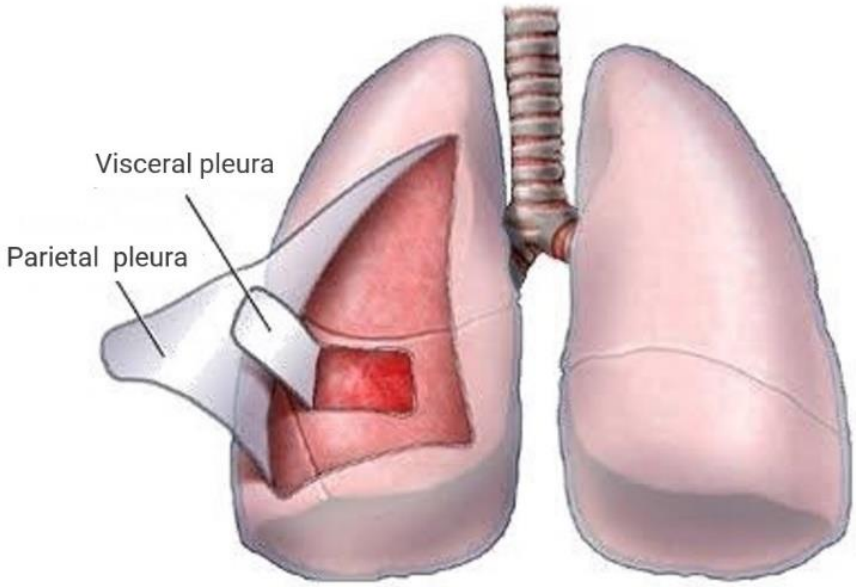

Fig. 3: Representation of lungs with visceral pleura and parietal pleura.

As already stated, breathing is possible thanks to the presence of the bronchial tree. The latter is created from an initial branching of the bronchi, which continue to branch further into smaller bronchi, which gradually change their structure, becoming smaller and leading to the generation of the terminal bronchioles. Each terminal bronchiole bifurcates into two respiratory bronchioles, on the walls of which are sac-like structures surrounded by a dense network of capillaries: the alveoli. The elementary unit of the lung parenchyma is the lung acinus, i.e. the set of all the branches that originate from a terminal bronchiole. In utero, immersed in amniotic fluid, there is no air. The fetus, therefore, does not breathe inside the womb, or rather, not as breathing is generally understood, but is oxygenated through the umbilical cord that connects the baby to the placenta. The first real breathing occurs only immediately after birth, thanks to the maturation of the lungs that occurs around the 36th week of pregnancy. Development of the fetal lung begins at six weeks gestational age and continues

until the second year of life. The lung develops through two main processes: the formation of the gas exchange units, i.e. the future alveoli, and their subsequent enlargement and multiplication. Both of these processes occur through the deposition of two proteins, elastin and collagen, and the reorganization of capillaries. Around the 25th week, there are fairly well-developed alveoli and type II pneumocytes that produce surfactant and continue to mature during gestation. The lungs continuously produce fluid, consisting partly of transudate from the pulmonary capillaries and partly of lung surfactant secreted by the pneumocytes. For the normal gas exchange that occurs at birth, the alveolar and interstitial lung fluid must be removed immediately. This elimination process occurs mainly through the absorption of fluid into the lung cells through the activation of epithelial sodium channels.

There are significant differences in the physiology of the respiratory system of infants compared to older children and adults; these are anatomical dissimilarities, which may account for the greater onset and severity of respiratory symptoms in the early years of life. It is important to understand what the dissimilarities are so that possible risks and pathologies can be assessed. An infant's nose is more vascularised, small, and flat, and this may be more conducive to upper airway obstruction [15]. The trachea and bronchi are thinner and poorer in cartilaginous tissue and therefore tend more easily to collapse, so children have more frequent episodes of asthma and asthmatic bronchitis than adults [5], and the chest wall is more easily collapsed. Furthermore, the smaller diameter of the infant's airways increases their resistance, and the absence of collateral ventilation increases the tendency for atelectasis, i.e. reversible collapse of lung tissue with loss of volume. Another important difference is the different respiratory rate, as in the newborn this can vary between 40 and 60 breaths/min, with a usually rhythmic pattern. Compared to an adult who breathes regularly, newborns, especially premature ones, may show a regular rhythm for about a minute, which may be

interspersed with pauses of up to 10 seconds. If this condition persists, one is no longer in a normal condition but is considered apnoea. The other components of breathing are similar for children and adults.

1.2. Surfactant

The proper functioning of the respiratory system depends on surface tension, which increases the lung's resistance to expansion and is determined by a layer of fluid between the alveolar cells and the air. To reduce this surface tension, at the level of the alveoli, the lung produces a substance known as surfactant, which is a mixture of phospholipids and lipoproteins secreted by type II pneumocytes. Some components of the surfactant, and also their effects, have been observed in the tracheobronchial tree, but they originate in the alveoli [6]. This substance prevents the alveoli from collapsing and facilitates respiration. In addition to ensuring proper surface tension, surfactant and its individual components silence inflammatory responses, bind and destroy airborne microbes, facilitate phagocytosis by alveolar macrophages, and bind endogenous and exogenous molecules [7]. The surfactant, composed mainly of amphipathic molecules, forms spontaneously stable films at the air-water interface of the alveoli, capable of drastically reducing the surface tension from around 70 mN/m in pure water at physiological temperature to almost 0 mN/m. The alveolar air-water surface is the site of surfactant's major effects on lung mechanism [8]. This is made possible by the fact that the polar groups of surfactant molecules establish polar interactions with interfacial water molecules and thus reduce net intermolecular cohesive forces [2]. The respiratory system is responsible for ventilation, which is ensured by the cyclic process of inspiration-exhalation and is also responsible for the gaseous exchange of oxygen and carbon dioxide between the atmosphere and the bloodstream at the level of the alveoli. This exchange of respiratory gases occurs through a relatively complex physical barrier, consisting of the thin aqueous film that lines the alveolus, the alveolar epithelial cells, the interstitial layer, the endothelial cells that form the blood capillaries, the blood plasma, and, finally, the erythrocyte

membrane. Due to the fluid coating inside the alveoli, which is a consequence of cell metabolism, the lungs have to cope with surface tension at the interface between the hypophasic fluid and air. [2]. To prevent lung collapse, therefore, especially at the end of the exhalation phase, type II pneumocytes, which are alveolar cells, secrete surfactant which is responsible for minimizing the mechanical forces that could cause collapse [2].

Indeed, in the absence of surfactant, the lungs are subject to high surface tension, which in this case can be assumed to be equivalent to the surface tension of plasma [9], and a collapse is inevitable.

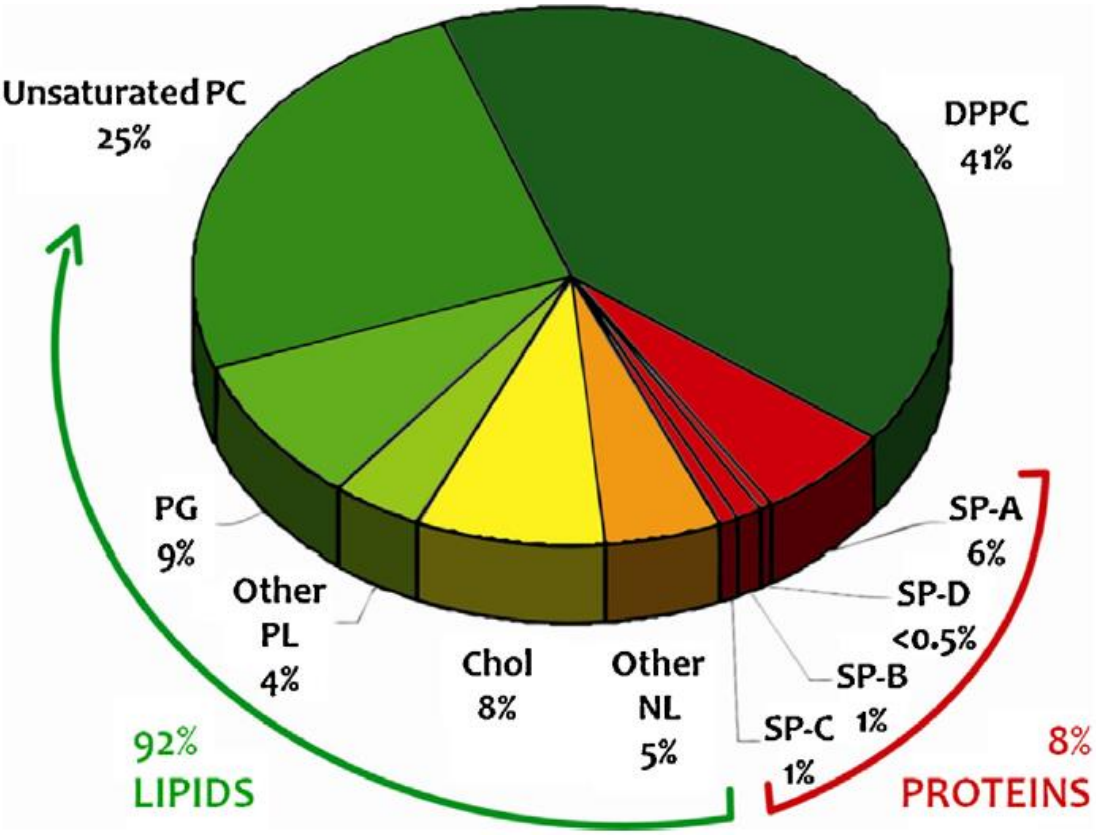

Fig. 4: Surfactant composition.

As shown in Fig.4, the surfactant is mainly composed of lipids, which account for about 90 percent of the mass, and several lipid species are present: phospholipids predominate (about 60-70 percent of the mass) and anionic species, which account for 8-15 percent of the total mass of the surfactant in mammalian lungs [2]. Surfactant is composed of several proteins, all of which are essential for proper activity within the alveoli. In particular, three of the four proteins present in the alveolar hypophase, SP-A, SP-B, and SP-C, but not SP-D, are membrane-associated and, although in small amounts that occur naturally in membranes, play crucial roles in surfactant function [2]. It must also be considered that the effects of surfactants in maintaining proper lung function are also related to the surfactant's absorption mechanisms [6]. Experiments have also shown that surfactant plays a role in increasing resistance in the case of contact with allergens [10], which may improve mucociliary clearance in the case of unwanted contaminants [11,12]. The alveolar surface tension reaches very low values during deflection of the lungs, reaching much lower values than 9 mN/m for about 30 minutes at 37° [13]. There is a linear relationship between surface tension and volume during lung deflation [13]. In vivo, experiments on large animals have made it possible to assess the surface tension in the large conductive airways directly using a video endoscope, based on the diffusion behavior of oil drops placed on the tracheal or bronchial walls. Low values of this voltage have been measured, which suggests the existence of a surface film in large airways [11]. In addition, a film is also in the lungs of smaller animals, capable of decreasing surface tension [14]. The same lipid and protein components, so the surfactant components appear in analyses of human and other mammalian species [6], with a lower amount in humans concerning the other species. The relatively small surfactant pools in humans may make the lungs more susceptible to injuries [8].

1.3. Respiratory Distress Syndrome

The adaptation from the intrauterine to the extrauterine life is a complex process, which generally occurs gradually and without problems in full-term newborns. In the case of premature infants, however, the immaturity of the organs and systems leads to problems in respiratory adaptation, which is necessary for survival. In some premature infants in particular, but also infants with a shorter-term frequency, a sufficient amount of surfactant is not produced. Hence the respiratory distress syndrome (RDS) condition, which is the leading cause of respiratory failure [15]. Surfactant production and function may be decreased in cases of prematurity, maternal diabetes, meconium aspiration by the newborn, and neonatal sepsis. Generally, the surfactant reserve in a full-term newborn is about 100 mg/kg, whereas in premature infants it may be extremely insufficient, with values ranging around 4-5 mg/kg [16]. A deficiency in the amount of surfactant produced leads to the inability in subjects to keep the alveoli open between one inhalation and the next; therefore, the alveoli tend to collapse, as shown in Fig. 5 and, to be expanded again, a great effort is necessary. This can then lead to conditions of hypoxemia, i.e. lack of oxygen and respiratory failure.

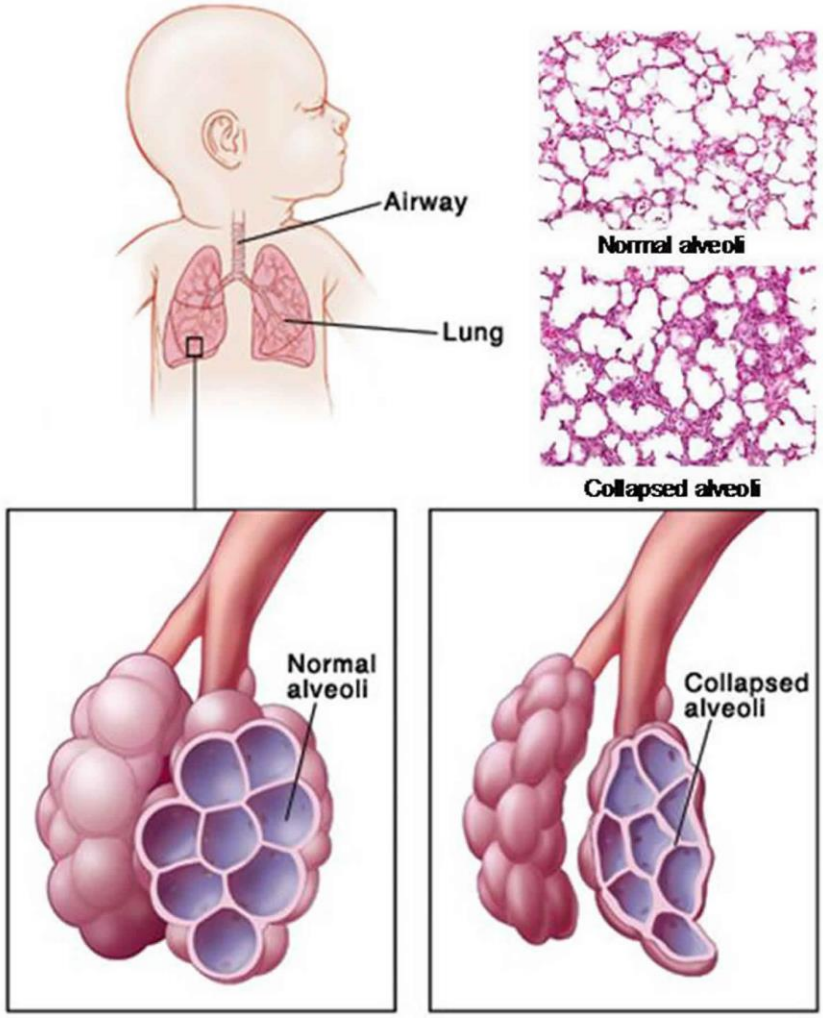

Fig. 5: Comparison between healthy alveoli and collapsed alveoli.

Several respiratory disorders arise from the imbalance between surfactant production and consumption [17]. RDS is one of the most common disorders that a preterm child may experience, and it is a syndrome that is generally inversely proportional to gestational age, or it becomes more acute the higher the level of prematurity of the newborn. RDS occurs in almost all children born between 22 and 28 weeks of gestation, in about 30% of those born between 28 and 34 weeks, around 3% of children born between 34 and 36 weeks, in less than 5% of those born over the 34-th week and only in 0,12% of cases in infants born after the 36th week of gestation [18,15]. Respiratory failure as a result of a lack of surfactant is the main

cause of morbidity and mortality in preterm births. Surfactant therapy reduces morbidity and mortality in these newborns. This syndrome occurs at or immediately after birth and symptoms worsen over time [19]. The manifestation of RDS is also due to genetic factors [20, 21], in fact, studies show that in males the development of surfactant in amniotic fluid is delayed compared to women, and this can lead to greater ease in contracting RDS [22]. The administration of surfactant therapy after birth to preterm infants improves the condition of RDS [18]. Proper treatment of neonatal RDS requires optimal respiratory support. Alveolar expansion must be maintained to ensure optimal oxygenation and good ventilation and can be ensured through external pressure administration [18]. The absence of surfactants in the liquid lining film of the alveoli causes an increase in surface tension and alveolar collapse [19]. Pulmonary atelectasis leads to a maladaptation of ventilation and a mismatch of perfusion, hypoxia and finally respiratory failure in newborns not treated with RDS [19]. Since most preterm infants with RDS require ventilatory support, BPD (bronchopulmonary dysplasia) is one of the main morbidities of many forms of ventilatory support, The hope is to find a safe and effective non-invasive RDS ventilation method [19]. The administration of surfactants followed by conventional ventilation is the most common choice, but it is feared that both CPAP through the endotracheal tube and the duration of mechanical ventilation have direct effects on the incidence of BPD [19]. CPAP is a form of continuous stress relief, which facilitates the maintenance of increased transpulmonary pressure throughout the respiratory cycle [23]. Several CPAP devices are available which can be divided into continuous flow and variable flow [23]. When positive pressure is applied to the airways of infants in spontaneous respiration, it helps to maintain residual functional capacity (FRC) and assist gas exchanges [23]. The FRC is the volume of air present in the lungs at the end of passive exhalation, and in this condition, the forces of elastic recall of the lungs and chest wall are

equal but opposite and there is no effort by the diaphragm or other respiratory muscles. The loss of FRC may be partially compensated by the application of CPAP to maintain lung volume and prevent ventilation/perfusion mismatch [23]. The nasal skin is important for optimal delivery of pressure and CPAP while limiting unwanted effects. requires close monitoring and good nursing [24]. CPAP, during breathing, increases pressure to overcome the resistance and elastic properties of the respiratory system. FRC is the amount of air that is present in the lungs immediately after exhalation, and in case of FRC abnormalities, the use of CPAP allows the lung volume to be maintained [24]. Oxygen can be administered using a nasal cannula or facial mask. In the continuous positive airway pressure, the pressure is kept constant throughout the respiratory cycle, to keep the alveoli open and improve oxygenation. An example of CPAP is continuous bubble positive pressure ventilation [25]. The CPAP technique can fail if the newborns subjected to it are affected by RDS, due to a lack of surfactant. Administration of the latter is therefore necessary [25].

Mechanical ventilation (MV) can potentially cause airway trauma, hemodynamic disturbances, and lung injury. BPD occurs due to the imbalance between immature lung repair and ongoing lung injury and inflammation [16]. The less invasive administration of surfactant involves the administration of the surfactant without endotracheal intubation. Several less invasive strategies in practice are:

(1) Administration of surfactant by thin catheters.

(2) Surfactant replacement therapy (SRT) with laryngeal mask

(3) Pharyngeal instillation of surfactant

(4) Nebulized surfactant

Observational studies have reported better long-term outcomes after more than 2 years of using the thin catheter technique [16, 26, 27]. Compared to the other methods for surfactant

administration, the thin catheter technique of surfactant administration seems to offer important advantages in terms of clinical outcomes [16].

Studies between 23 and 34 weeks of gestation show that surfactant reduces lethality and the incidence of more dangerous diseases. Surfactant has also proved useful in more mature preterm with respiratory difficulty syndrome because it reduces mortality [28].

Fig. 6: Endotracheal system for surfactant delivery.

There are several techniques for surfactant administration, such as LISA (Less Invasive Surfactant Administration) or INSURE (Intubate Surfactant Extubate). In the first case, the aim is to maintain spontaneous breathing, that is, to provide a dose. At the same time, the newborn breathes spontaneously, thus avoiding intubation and the support of positive pressure

ventilation. In contrast, the second method is used through intubation of the patient and a subsequent period of positive pressure ventilation. In particular, the LISA technique allows patients, who are preterm infants, to benefit from spontaneous breathing [29]. However, the INSURE method was also found to be effective in improving respiratory failure, in particular early surfactant administration, in combination with CPAP, provided optimal results. The combination of the two above techniques was found to be more effective in improving oxygenation and reducing respiratory disease [30]. Surfactant administration can be prophylactic (or preventive) when done within 30 minutes of birth in infants at high risk of RDS, to prevent such disorder. Otherwise, it may be administered as therapy in case of clinical evidence of RDS [28].

Administration is through an endotracheal tube, inserted into the trachea, both as a bolus and as a continuous infusion. Oxygen desaturation often occurs during administration, more frequently with bolus administration. It can be said that it reduces the incidence and severity of RDS and the mortality of preterm infants [28]. It has been shown that the administration of the surfactant in the early stages of respiratory distress, therefore before the 2 hours of the life of the newborn, is preferable to a delayed administration for subjects requiring mechanical ventilation, as it reduces the risk of complications such as pneumothorax [18].

As previously stated, nebulization is another less invasive surfactant replacement therapy method. It must be considered that endotracheal intubation, followed by mechanical ventilation, is an effective solution but it involves risks for the patient, such as injuries in the airways at the level of the pharynx. For this reason, spraying can be considered a valid alternative, in which the administration of the surfactant no longer takes place in the form of a bolus, but the medicine is broken down in the form of particles traveling through the airways.

1.4. Nebulization system

Surfactant therapy plays an essential role in the management of RDS as it reduces pneumothorax and improves survival. However, intratracheal administration requires skill and may cause harm, particularly if uncontrolled positive pressure is applied to the newborn lung. Before 2013, prophylactic surfactant was recommended for the smallest babies as it improved survival in clinical trials from the pre-CPAP era. After 2013, with increased use of antenatal steroids and early initiation of CPAP, outcomes are best if surfactant is reserved for infants showing clinical signs of RDS, and for the smallest infants early initiation of CPAP may avoid the harmful effects of intubation and mechanical ventilation (MV) during the transitional phase. The overall aim is to avoid invasive MV if possible whilst endeavoring to give surfactant as early as possible during RDS once it is deemed necessary. Different devices were developed for aerosol generation, such as pressured metered-dose inhalers (pMDI), small-volume nebulizers (SVN), and dry powder inhalers (DPI) [32]. The pMDI is a small device that dispenses multiple doses of drug by a metered value, but this device is not widely used because of difficulties due to the dispersion of the pharmaceutical inside the oropharynx [32]. SVN aerosol generators convert liquid drug solutions to an aerosol. These devices can be powered by air compressors or other sources. [32]. DPI delivers the drug in a powdered form [32].

Nebulizers are currently used for pharmaceutical delivery to patients since they are safer and less harmful.

The spray therapy requires devices that can administer a sufficient dose of medicine, in this case, surfactant, in a short time, and efficiently to reach the target. Although it may be an effective solution, most nebulizers fail to reach the lower airways. Therefore, the medicine

does not reach the lungs, since lung deposition may range from 1% to 50% in the clinical application [32], as only 10 % of the dose generally reaches the target [31].

Nebulizers generally used for the administration of medicines produce an aerosol in which the medicine is dispersed in small particles, with a diameter of 1-5 µm, generally pushed in most cases by compressed air (Fig. 7 others use ultrasonic waves (Fig. 8). A nebulizer differs from an atomizer in that the first removes particles that are too large [31], while the second produces larger particles. Initially, the nebulizers were atomizers, which were gradually upgraded to filter particles with a diameter greater than 5 µm.

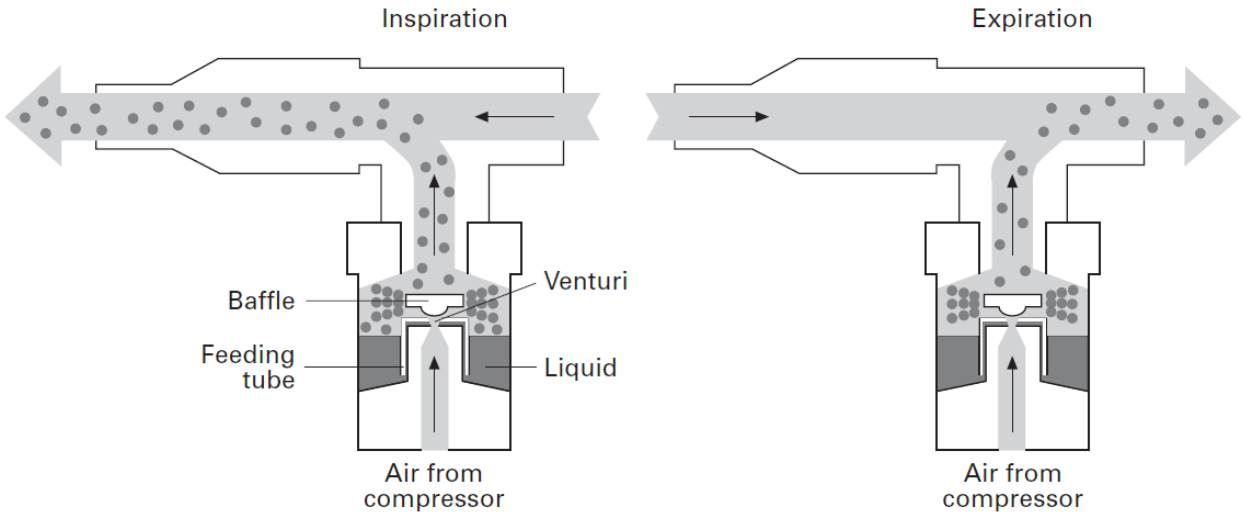

Fig. 7: Representation of a pneumatic nebulizer [31].

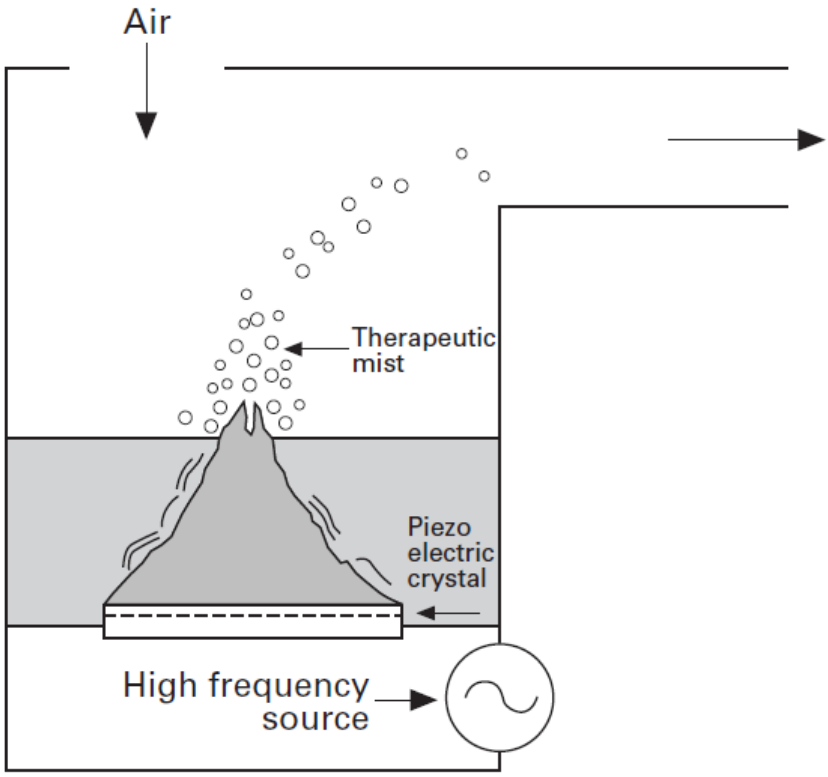

Fig. 8: Representation of an ultrasonic nebulizer [31].

The type of nebulizer shown in Fig. 7, most commonly used, is the Pneumatic Nebulizer: the medicine passes through a very narrow opening with initially high pressure. Once through the opening, the pressure decays, and the particles are accelerated. This type of device exploits the Venturi effect by which a fluid forced to pass through a reduced space, a bottleneck, undergoes a decrease in pressure and an increase in speed. The fluid is then found to pass through a narrow tube, creating a collapse of pressure that pulls out the fluid in the form of ligaments. These ligaments collapse rapidly into droplets due to the surface tension of the environment, thus generating particle atomization of 15-500 microns [31].

These particles, which are still too large to reach the lower airways, impact deflectors (baffles), while smaller particles are inhaled or impact the walls of the tissues and are

nebulized again. This principle, however, results in poor output, as most particles impact baffles and walls. So recent studies are investigating the design of new systems to optimize this problem. A possible solution was found by adding an extra valve in the system: this opens during the inhalation phase, increasing the amount of air and then the amount of nebulized fluid, while closing during exhalation, removing air and reducing the amount of fluid released. The Ultrasonic Nebulizer instead uses a piezoelectric crystal that vibrates at high frequencies to produce aerosol particles. Vibrations are transmitted from the crystal to the surface of the fluid, generating wavefronts, and droplets are generated by detaching from the crests of the wavefronts. As for pneumatic nebulizers, there are baffles in ultrasonic nebulizers that remove particles that are too wide. These particles fall back into the drug reservoir and are nebulized again.

The particle size during the evaluation of the mist is indicated by considering the droplets' surface to be spherical. In particular, reference is made to diameter, precisely the parameter used for particle classification is mass median aerodynamic diameter (MMAD) [31]. The following figure shows the diameter characterizing particles in different levels of airways.

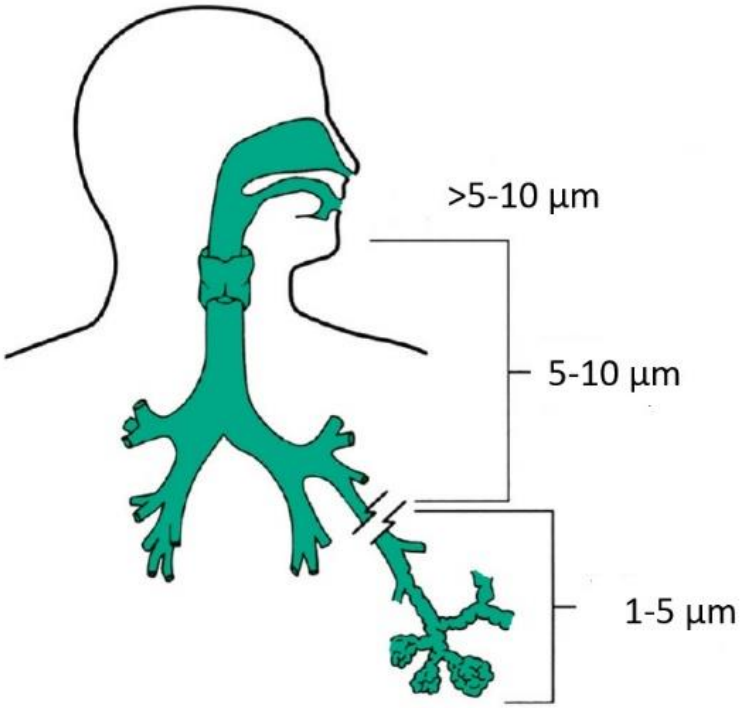

Fig. 9: Difference in particles dimension along the airways.

This study will analyze the performance of a pneumatic-type nebulizer, aimed at spraying surfactant intended for premature sufferers of RDS.

Chapter 2: Materials and Methods

2.1. Measurement setup

The aim of this study consists of examining a nebulization system for surfactant drug delivery. In order to investigate all the processes involved in the nebulization mechanism, a proper measurement setup was created, with a series of connected components able to simulate the nebulizing activity. All the several components necessary for the creation of the previously enunciated measurement setup are later shown, in Fig. 10.

A prototype for the administration of nebulized surfactant drug via pulmonary trigger has been realized in the laboratories.

The main component of the overall device system consists of an element that allows two capillary catheters to be coupled and organized in a coaxial structure. With this configuration, it's possible to have both the surfactant and the compressed air carried close to the distal part of the catheter thus corresponding to the trachea. Briefly, the catheter with the surfactant is positioned to pass inside the air tube and then deposits a small drop at the end of the capillary that will be atomized by the airflow. The amount of surfactant is managed by a syringe connected to a motorized linear guide and programmed to feed a specific amount of drug into the circuit. Finally, the compressed air is supplied via a solenoid valve with pressure and time control. A schematic representation of the measurement setup is shown subsequently, in Fig.11.

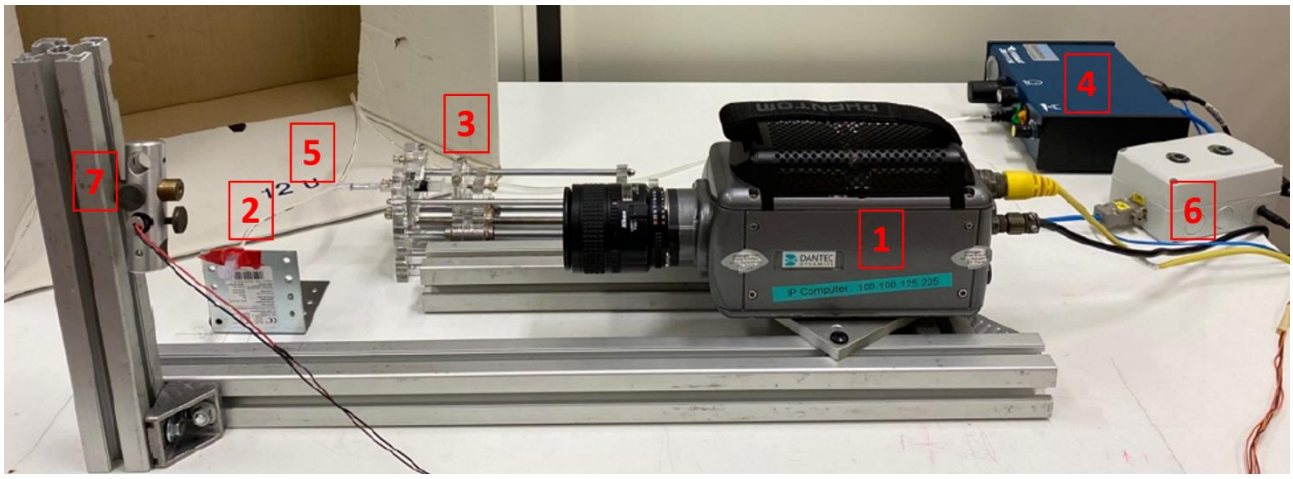

Fig. 10: Measurement setup. 1: speed camera; 2: Nebulizer; 3: Syringe; 4: Valve; 5: Connector; 6: Control Unit; 7: Laser.

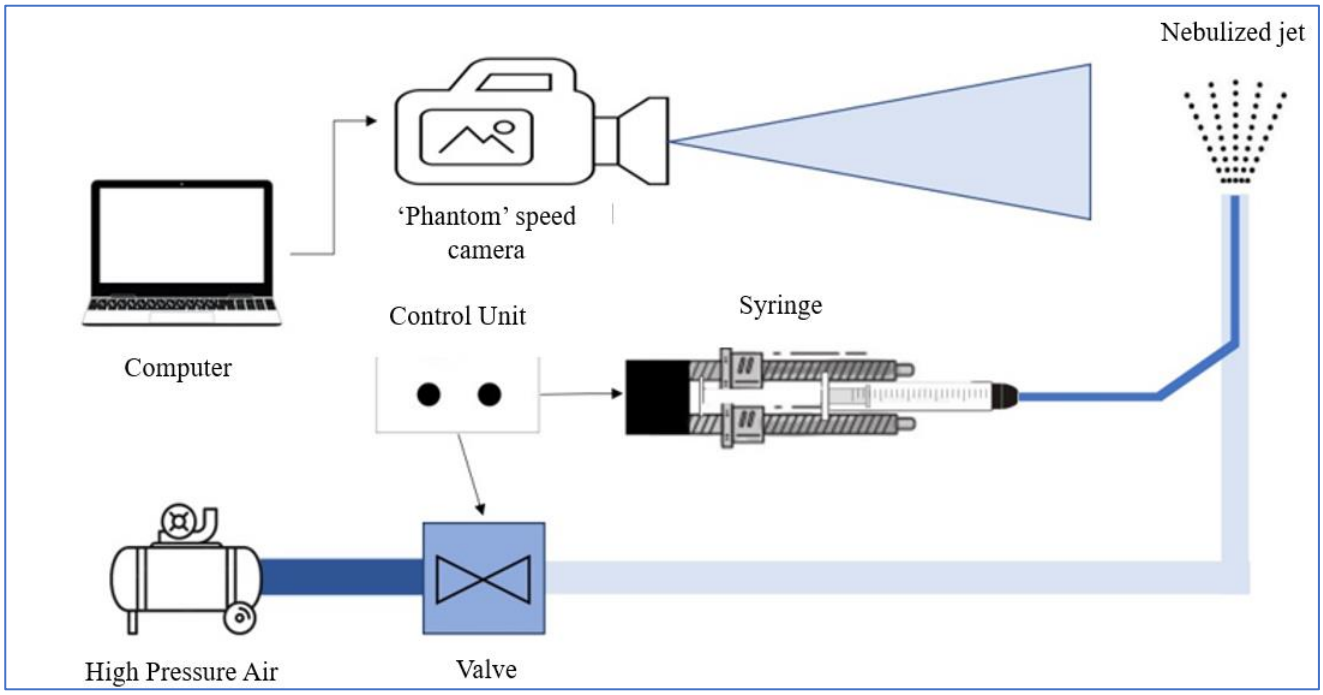

Fig. 11: Scheme of the measurement setup.

All the components in the measurement setup are:

- The camera.
- The nebulizer.
- The syringe.
- The electro-pneumatic valve.
- The connector.
- A control unit.
- The control interface.

The explanation of all the previously stated components will start with the camera.

It is a Phantom V10 speed camera, for the slow-motion acquisitions, which has been positioned on a guide system, as shown in (1) in Fig.10 to ensure its position in a fixed point. The choice of maintaining a fixed position is due to the necessity of having a constant distance between the camera's lenses and the nebulization tool. This approach ensures that calibration is performed only once and also the focusing adjustment must not be repeated for each acquisition during the measurement phase. In particular, calibration and focalization were performed only one time at the beginning of each measurement session, when the camera was switched on. The acquisition procedure settings were regulated using specific software, from which several parameters could be set. The camera's task consisted of acquiring the surfactant jet ejected by the nebulizer, thanks to the small mechanism to which it was connected. The electro-pneumatic valve, shown in (4) in Fig.10, and more in detail in Fig.12, was connected to compressed air, which was necessary for the ejection mechanism. Indeed, the valve produced an output that consisted of an air ejection that was sent toward the nebulizer, thanks to specific connections. In particular, on the interface of the electro-pneumatic valve, it was

possible to regulate the two parameters of pressure (bar) and blowing time (seconds, s). These adjustments are necessary to regulate the amount of air delivered to the nebulizer, together with the drug that needs to be nebulized. The control unit, operated by a push button, governs the functioning of both the valve and the syringe.

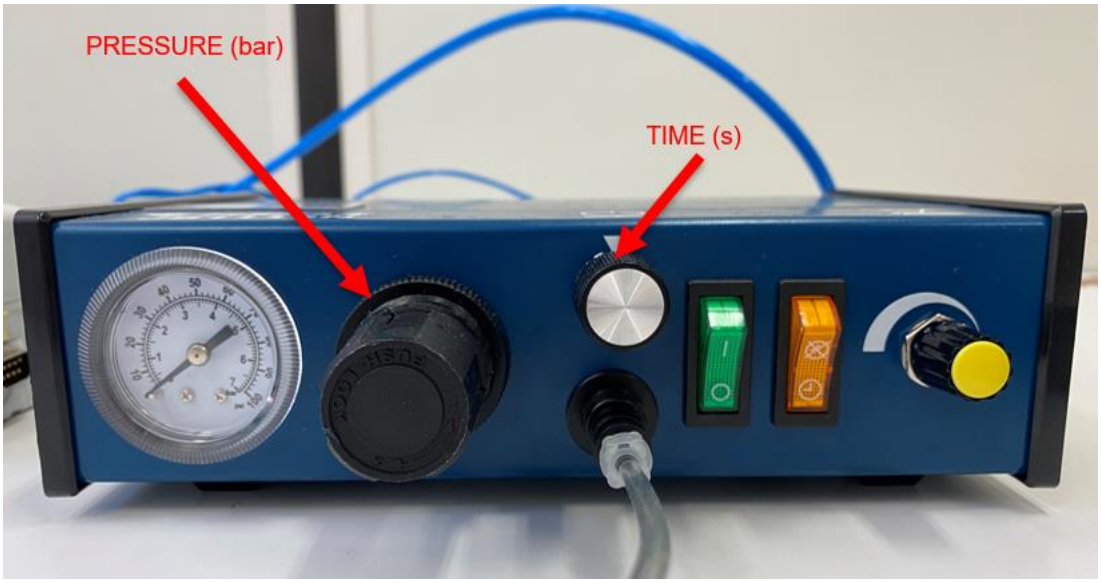

Fig. 12: Electro-pneumatic valve.

The syringe is shown in Fig.13, and its position is (3) in Fig.10, was responsible for the delivery of the surfactant drug to the nebulizer. It was mounted on a rigid, metallic guide, with a structure in such a way that it could be actuated by the control unit. On the back side of the guide, there was an actuator, linked to the control unit. Upon activation, the actuator pushed the syringe in the forward direction to eject a certain dose of surfactant, previously defined by the producer which designed the nebulizer. Indeed, on the edge of the nebulizer was already present the decided dose of surfactant, which after the input provided by the control unit, was nebulized following the initial parameters previously set on the electro-pneumatic valve.

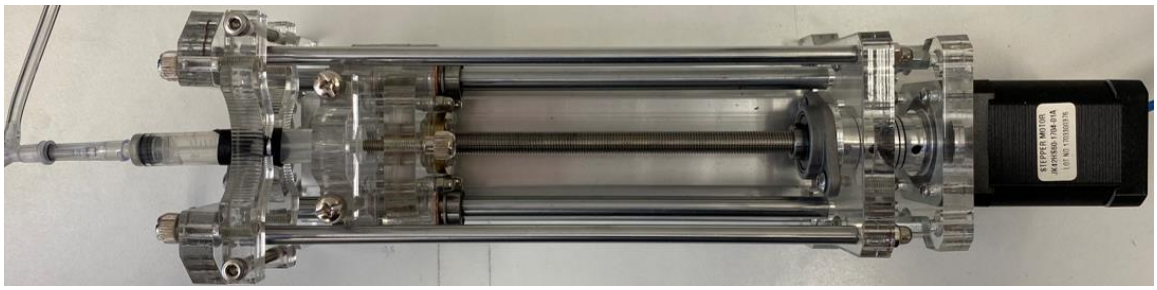

Fig. 13: Syringe placed on the guide and actuator.

The dose was set up using a user interface (Fig.14). The syringe system was connected to the electro-pneumatic valve system using a specifically modified connection.

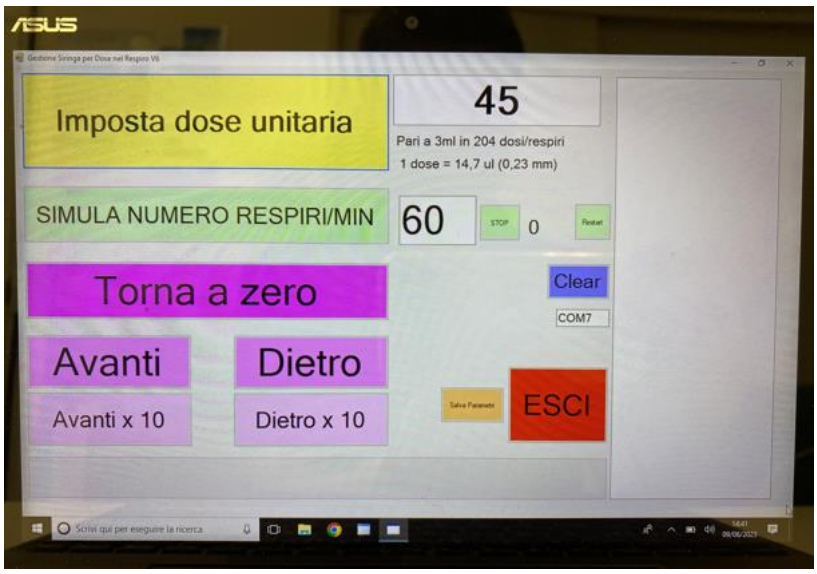

Fig. 14: User interface.

In particular, the used connector consisted of a modified T-shape connector able to combine two different outputs. The connector, (5) in Fig. 10, is better illustrated in Fig.15, and it has a coaxial structure. The inner tube contains the surfactant, and the outer tube, linked to the electro-pneumatic valve, serves as the pathway for compressed air. So, the control unit performs a synchronization between the syringe and the electro-pneumatic valve actions, and the result of the ejection is recorded using the speed camera and later stored on the computer. Fig.16 illustrates the setup of the tool used for the realization of the coaxial catheter is structured with a T-shape, wherein one of the extremities there is the surfactant drug capillary

tube, while in the other one, there is the tube associated with the compressed air ejected by the valve.

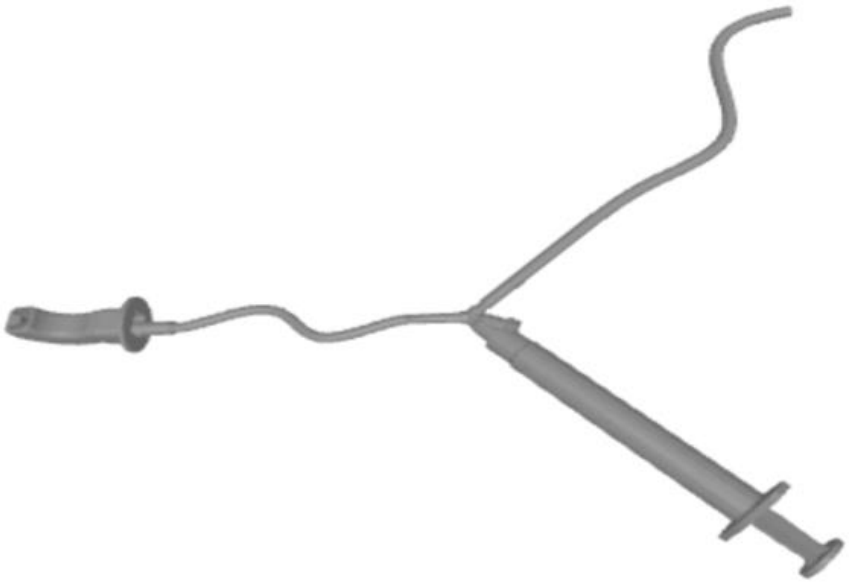

Fig. 15: T-shape modified connector.

Fig. 16: Device for the creation of the coaxial catheter.

The final component of the cycle is the nebulizer (2 in Fig. 10), which is displayed in Fig.17 and Fig.18. This small tool is fixed on a support, in a fixed position, to maintain a constant distance from the camera. The device must be considered as part of the endotracheal system that is used with the ventilator. The nebulizer receives the surfactant from the syringe, pushed by compressed air with the settings regulated on the valve. This component produces as output the nebulized ejection.

Fig. 17: Nebulizer.

Fig. 18: Model of the nebulizer.

All the acquisitions were performed using a red laser, shown as (7) in Fig. 10, with a wavelength of 650 nm, which produces a slice of light to acquire a plane.

2.2. *Acquisition and test parameters*

The objective was achieved by several videos of nebulization actions. To determine the optimal condition between those that were considered, some parameters. Two different types of analysis were conducted: the first one aimed to identify properties of the ejected particles, to determine which is the optimal parameter configuration for surfactant nebulization; the second one aimed to investigate the volumetric distribution of the several particles around the point of nebulization, immediately after the ejection. Regarding the chosen acquisition parameters, one main difference between the two analyses is represented by the decision to consider two different values of frame per second (fps) acquired by the speed camera during each video acquisition. More precisely, for the first step of analysis performed during this study, the camera was set to acquire 1000 fps, since the different measurement tests were performed in the natural light; during the second step of the analysis, tests were performed in the dark light, so it's been decided to set the camera to acquire 400 fps. The resolution during the work was 970x720 pixels and the used photographic lens was 60 mm. As already mentioned, the overall analysis consisted of two smaller analyses, where the first was preparatory for the second one. During the first step of the global analysis, initial investigations were conducted using water as the fluid for the nebulization. This choice was linked to the necessity of the implementation of a code for the examinations. More accurately, 60 trials were conducted with water, during which the code was finished, and then a total of 45 acquisitions with surfactant were performed, after which the code was adjusted. The test parameters are the quantities that are modified to evaluate which is the optimal parameter configuration for the present aim. The considered test parameters were the pressure, the blowing time, and the dose. The last one was kept constant, while the first two were

changed to have different combinations: pressure was set to 1,2, and 3 bar, while the blowing time was set to 0,2 and 0,3 S. To clarify, the initial combinations of pressure and blowing time amounted to six, as illustrated in the table 1 below.

Pressure [bar]	Blowing Time [s]	Dose [µl]	Number of acquisitions
1	0,2	14	10
1	0,3	14	10
2	0,2	14	10
2	0,3	14	10
3	0,2	14	10
3	0,3	14	10

Table 1: Measuring protocol for water analysis.

However, the configurations with pressures of 1 bar and 2 bar, along with a blowing time of 0.2, were excluded during analysis with surfactant.

Nebulization videos were acquired using a laser to allow the illumination of a single millimetric portion of the nebulized jet, to understand the particles behaviour at different position with respect to the origin of the nebulization. Videos were principally registered with the laser pointing in the centre of the nebulizer, and then at 2 mm and 3 mm from it, to have a volumetric representation. The laser has only been displaced in one direction forward the centre of the nebulizer, because of the hypothesis of symmetry with respect to the centre of nebulization.

2.3. *Measurement protocol*

Pressure [bar]	Blowing Time [s]	Dose [µl]	Number of acquisitions
2	0,2	14,7	15
3	0,2	14,7	15
3	0,3	14,7	15

Table 1: Measuring protocol for surfactant analysis.

The analysis was conducted by following the protocol shown in Table 2. For each combination of test parameters, 15 acquisitions were performed and later analyzed.

The main steps of the measurement protocol included:

1. Arrangement of the measurement setup
2. Performance of the measurement
3. Adjustment of the acquired video
4. Storage of the acquisition

During the first step, it is necessary to organize and prepare the measurement setup: the syringe must be filled with the surfactant drug, and once this action is completed the catheter must be inserted into the nebulizer; the pressure and the ejecting time are set on the valve; the dose is regulated through the dose adjustment program. Once all the parameter devices are organized, the system must be calibrated using the software and the next step is available.

The second phase of the process consists of the performance of the measurement, so it is the part in which all the videos are acquired. The acquisitions are obtained by following the

measurement protocol shown in Table 1, where fifteen videos for each different configuration of pressure and blowing time are obtained to be later analyzed. From the speed camera software, the parameters of the acquisition are set, so the frame rate (fps), the exposure time, and the resolution. Once these are fixed, the acquisition for the subsequent analysis is performed, by starting the recording of the video and simultaneously activating the ejection of the air and of the surfactant using the trigger.

The videos are then opened in the software MATLAB, to elaborate all data. During this part of the whole process each video is singularly checked, to evaluate the quality of the acquisition.

During the last step, all the acquired videos are stored for later analysis.

For the performance of the analysis, the particles have been considered circular shaped, and those identified as too small or too slow were considered outliers.

2.4. *Calibration*

As already anticipated, the purpose of this study is the effectuation of the analysis of the system previously explained. The analysis consists of the investigation of velocities and dimension distributions of the particles ejected during the nebulization. To have correct unit measures a calibration grid has been implemented. The calibration grid has been used at the beginning of the analysis to switch from the pixel unit measure description of the system to the description of the investigated quantities using the physics unit measures: meter per second (m/s) and millimeters (mm).

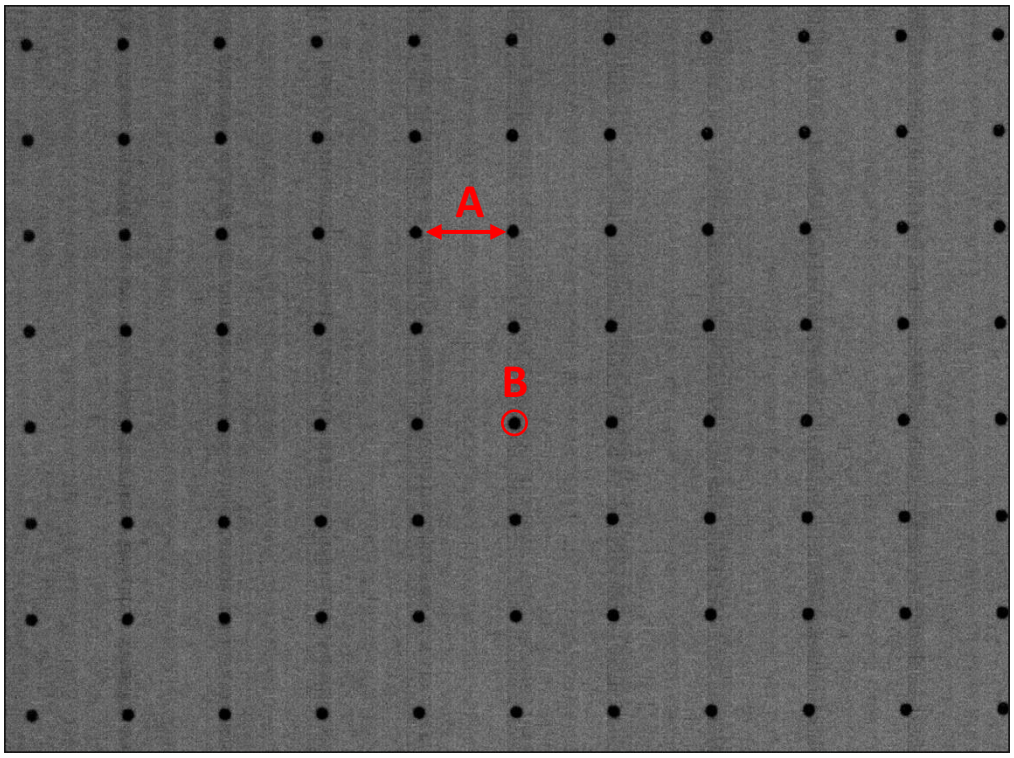

Fig. 19: Representation of the conversion grid. 'A' represents the computation of the distance between points; 'B' is the diameter of each point.

Thanks to the grid it's been computed the distance between the two consecutive points along each line, (A) in Fig. 19, and the diameter of the darker points of the grid, (B) in Fig. 19. In the end it resulted

A generic grid has been taken into consideration, with known measures. In particular, the already known quantities were the diameters of the darker dots and the distance between the two of them. Then the grid was compared with the MATLAB software representation, and the corresponding pixels were counted. In the end, it resulted that the distance between the darker points, which was known to be 5 mm, corresponded to 100 pixels, and the diameter of each darker point, which was 0,5 mm, was equal to 10 pixels.

2.5. *Data analysis*

2.5.1. *Creation of the tracker*

The performance of the overall analysis has been effectuated thanks to the creation and development of a tracker for the identification of the particles and the evaluation of their velocities and dimensions. All videos have been acquired by setting the parameters, and for each configuration, they have been analyzed.

The developed tracker consists of several steps: it starts analyzing the particles in each acquired video, and then it proceeds by analyzing the whole velocity distribution of the particles for each configuration, and so the dimension distribution. For the first step of the analysis, the videos were acquired with a sampling frequency of 1000 frames per second (fps), an exposure time of 900 μs, and a resolution of 960x720, and the parameters of pressure and blowing time were set at different values.

Each video was saved and, one at a time, was uploaded on the software MATLAB. Then the video was named, and the range of interesting frames was selected: videos were analyzed only in the part where the nebulization process was presented, so the frames associated with the beginning and the end of nebulization were identified. Steps of the tracker algorithm are shown in Fig. 20. In Fig. 21 an example of an acquired frame is displayed.

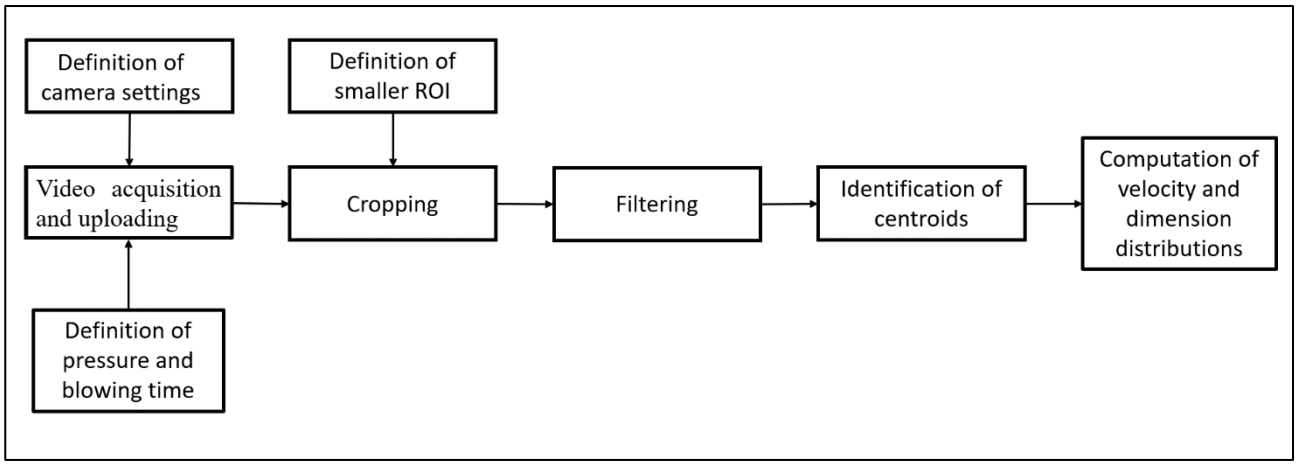

Fig. 20: Block scheme of the steps of analysis.

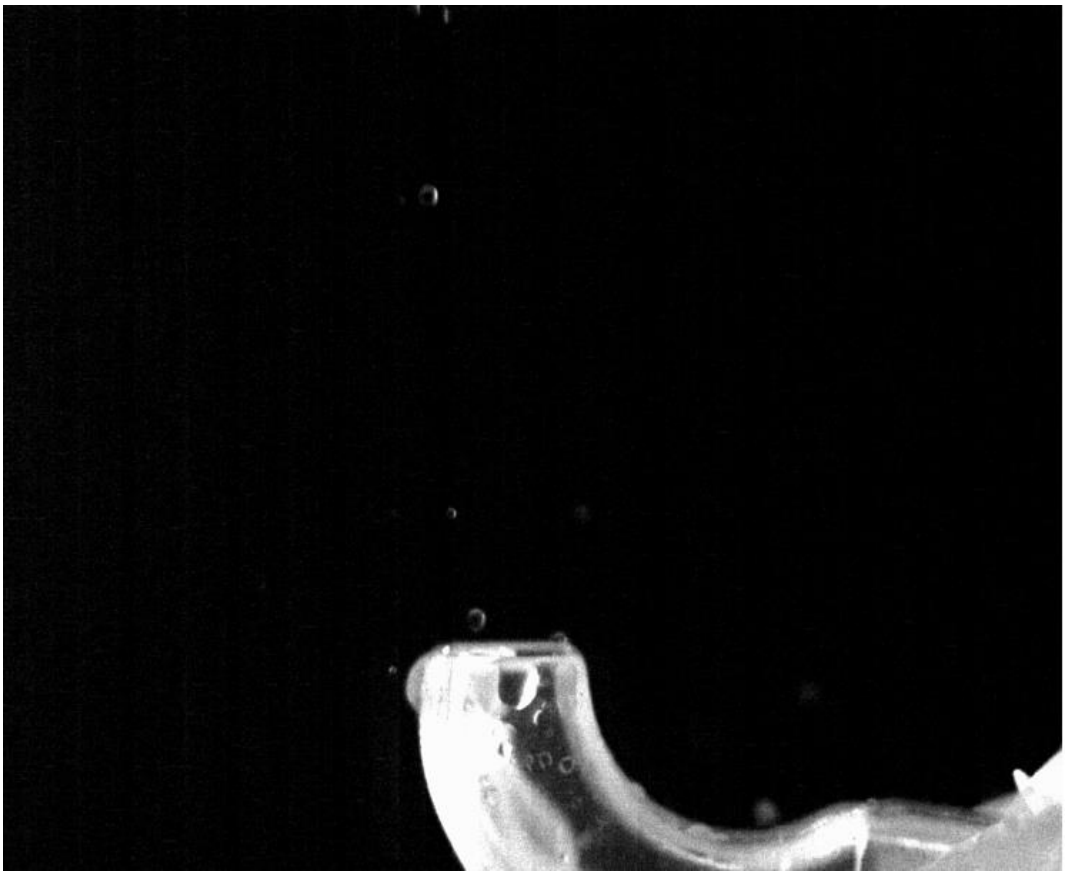

Fig.21: Representation of acquired frame.

A smaller rectangular region of interest (ROI) was defined to remove the image of the nebulizer from the analyzed field, as shown in Fig.22, since it could be an obstacle for the identification of the ejected particles, to maintain the portion of the image in which only the particles are present.

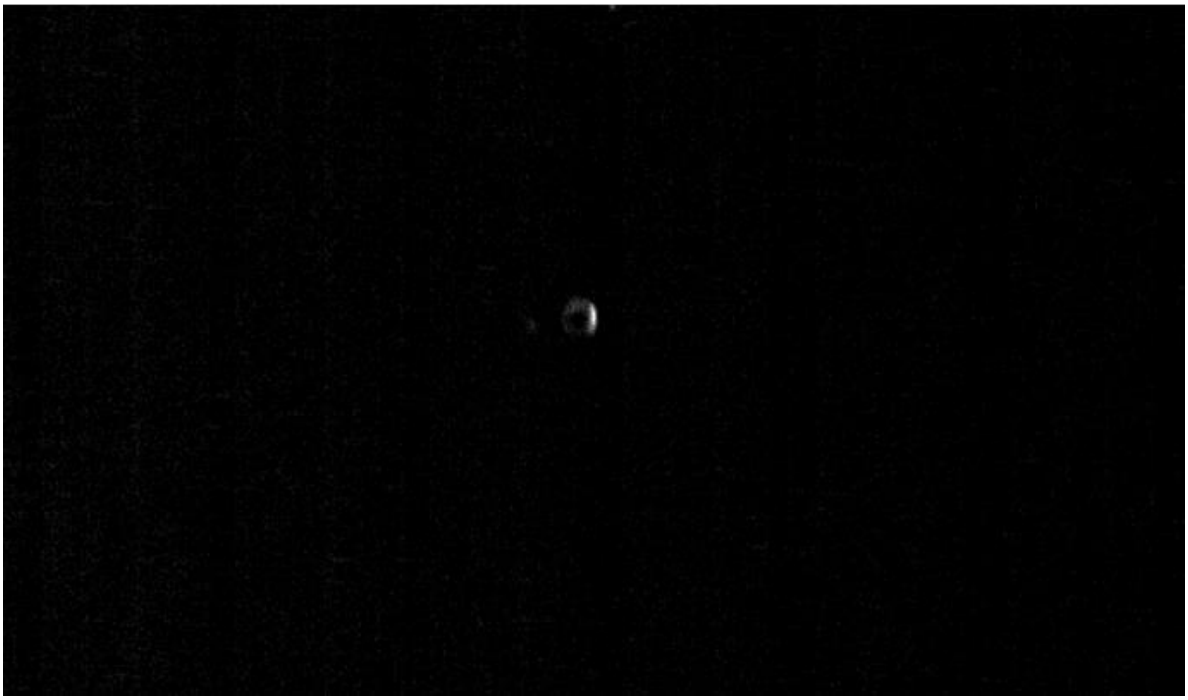

Fig. 22: Cropped frame.

A cycle was used to process a sequence of video frames within the specified range. The cycle reads consequently all the frames in the considered interval, denoted by an index, and each frame is cropped in the ROI previously defined. Then, the frame is filtered using an expressly created function, where a frame is considered as input and some image processing operations are performed on it. First, values of the frame are converted into double and divided by 255, which means that normalization is performed, to convert to the range [0 1]; a median filter is then applied to reduce the noise; the intensities are adjusted through a function which enables

to regulate the contrast. After that, a morphological closing operation of the previously adjusted frame is was performed for the closing of small holes in the image. To conclude the filtering, a Gaussian filter is applied for the smoothness of the image. In particular, the frame corresponding to the current index and the successive one, are cropped and filtered. The previous steps of the code consist of the identification of the necessary frames and their cropping and filtering processes.

After those passages, the real tracker is initialized. All the particles are supposed to be circular, so the tracking starts by identifying the position of the centers of all circles in the filtered images, with the additional option that allows the identification of circles with radius in the specified range. For the first acquisition performed using water, to establish the function of the tracker, the considered range was [1 5], while for the surfactant nebulization analysis, it was considered a range [1 30], since bigger particles were produced with respect to the water. After the determination of the centers, if these were larger than 0, their X and Y coordinates were saved. Since for each frame several particles were identified, procedure was iterated to each found particle. This tracker defines a region around each particle, so a smaller ROI with dimension 30x30 pixels, and then extracts binary images and detects the connected points inside them. It then identifies the centroid of the connected components corresponding to the considered particle, and tracks the particles from the current frame to the next one using a point tracker. The velocity is then computed by identifying the displacement in both directions, and by computing the difference in the centroid's positions between the two different frames. Once displacement is computed, the velocity is evaluated by dividing the space displacements for the time interval. The detected particle's velocity is stored in a previously defined velocity vector, after being multiplied by a conversion factor to have the final result in m/s. During the cycle, with the identification of the centroids, the dimensions

of the particles are evaluated too, and saved into three previously expressly defined vectors. So, in conclusion, the information about the centroids, dimensions, and velocities are iteratively stored in a structure array. The computed velocities are shown for each iteration, as shown in the following Fig. 23, with an arrow indicating the direction and the module. An empty vector is created for the storage of all the velocity values, extracted by the previously created structure array. A cycle is started and iterated over each element of the structure. More precisely, for each element, the corresponding velocity value is extracted from the structure and is appended to the vector, so at the end it will contain all the velocities of all the identified particles in the different frames, concatenated in a column vector. This process is done to create a dataset that combines information from multiple frames for further analysis. The whole previously enounced process is repeated for every single video, and the associated data are saved as a MATLAB file (.mat).

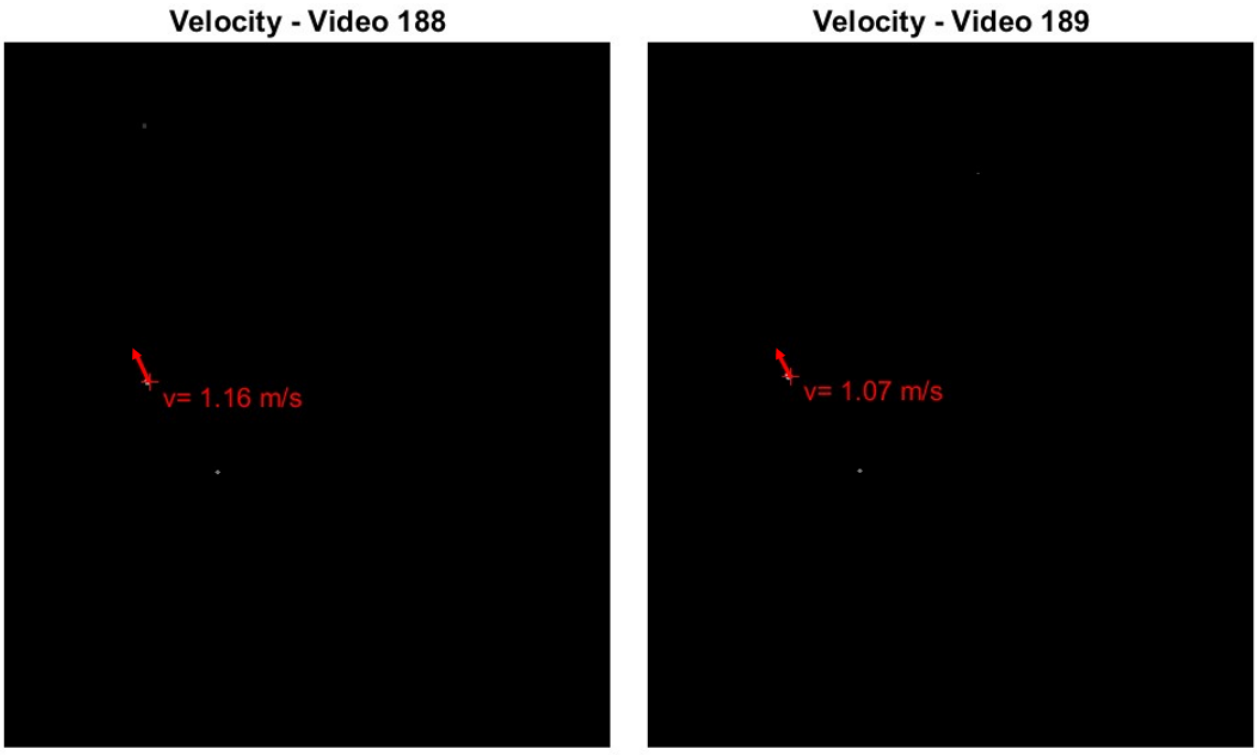

Fig. 23: Representation of the tracked velocity in two consecutive frames.

As can be seen in Fig.23, it’s possible to see how in two consecutive frames the velocity of the same identified particle decreases, because of the action of the gravitational acceleration towards the floor.

2.5.2. *Velocity and dimension distribution*

The tracker was created for the identification of velocity and dimension distribution to understand the best combination of pressure and blowing time to use for nebulization. Once all videos for all configurations were acquired and stored, they've been analyzed.

All data from videos in the same configuration were singularly saved, so for the analysis performance another code was created in which data from multiple MATLAB '.mat' files are organized in a single data matrix. A list of all desired files, associated to acquisitions of the same configuration, is created. During the cycle, data from the file are loaded and concatenated inside the matrix, made of four columns: the first two columns are the x and y coordinates of the identified centroids, the third column is containing the velocities, and the last column is for the dimension of particles. Since the first analysed parameter of the particle is the velocity, the third column is selected.

For the analysis, the first and second columns elements which are greater than zero are selected to eliminate all the outliers, so to exclude all particles that have a dimension lower than zero, because these quantities could be associated with noise grains present in the image because of disturbances in the measurement environment, such as for example the interference given to the light system in the laboratory. The matrix is filtered with a Gaussian filter, to obtain a chromatic representation of the nebulized jet, with a colour scale varying with the velocities of the particles. An example of the obtained image is displayed in Fig.24.

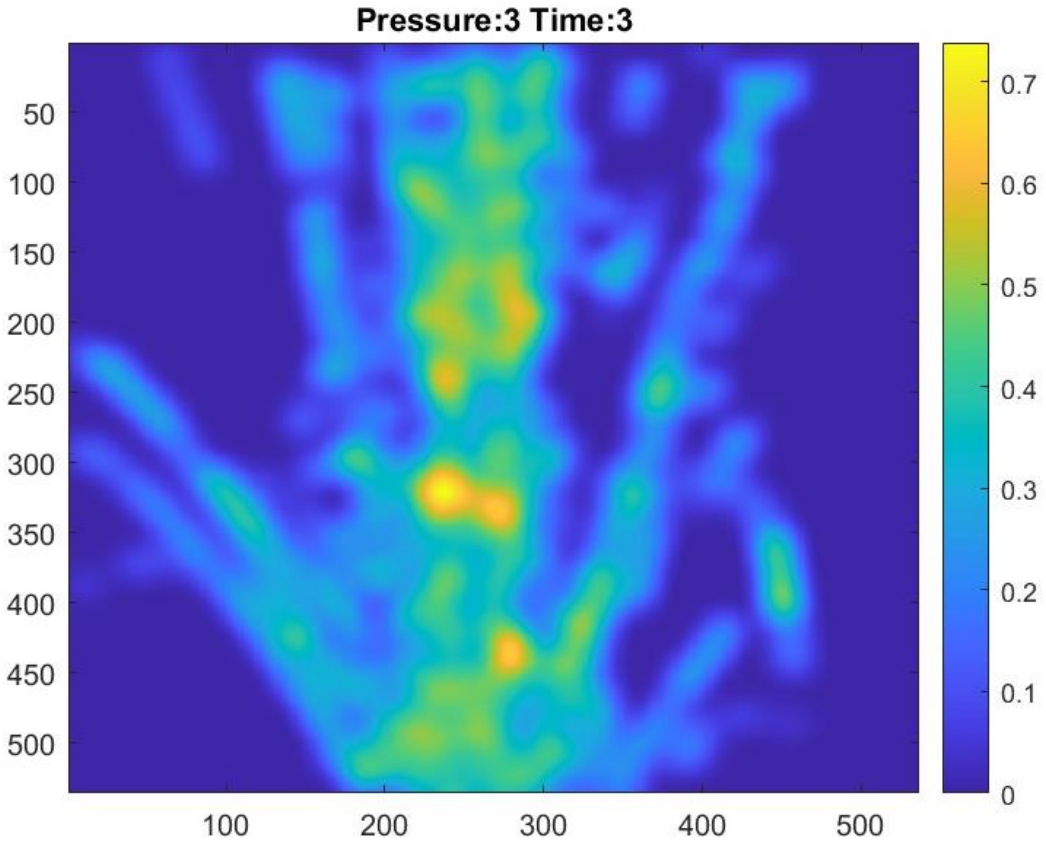

Fig. 24: Example of the chromatic representation of the nebulization, for the configuration with pressure of 3 bar and blowing time of 0,3 s.

The same analysis has been performed for all the considered combinations of pressure and blowing time, so to evaluate the efficiency in a first visual differentiation of the velocity distributions. In particular, the colour bar has been set with the same upper and lower limits to evaluate differences in the different configurations.

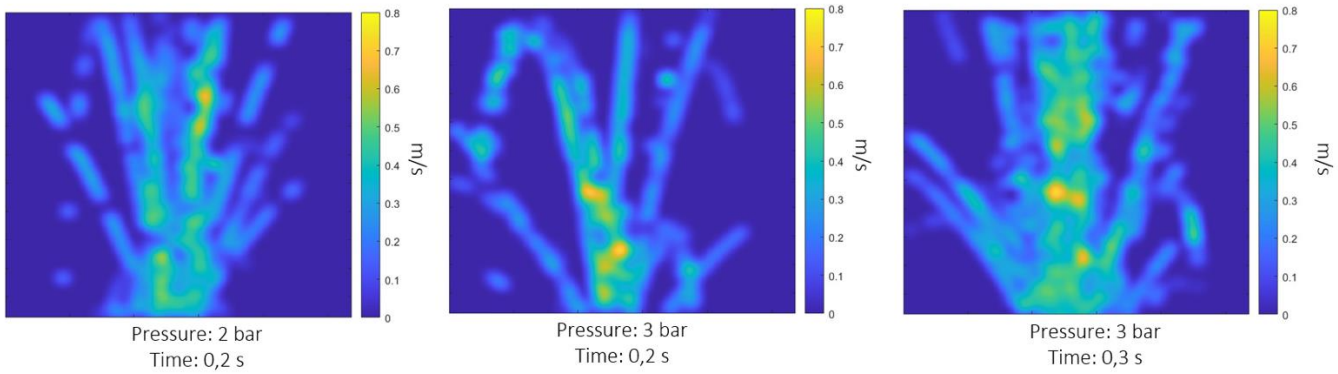

Fig. 25: Chromatic Representation of the different configurations of Pressure and Blowing Time.

After the elimination of the outliers and the definition of the correctly filtered image, the velocity analysis has been performed in different regions around the nebulizer end.

Four regions have been defined (Fig. 26): two of them were placed in the central part of the image, while the other two were in the side parts.

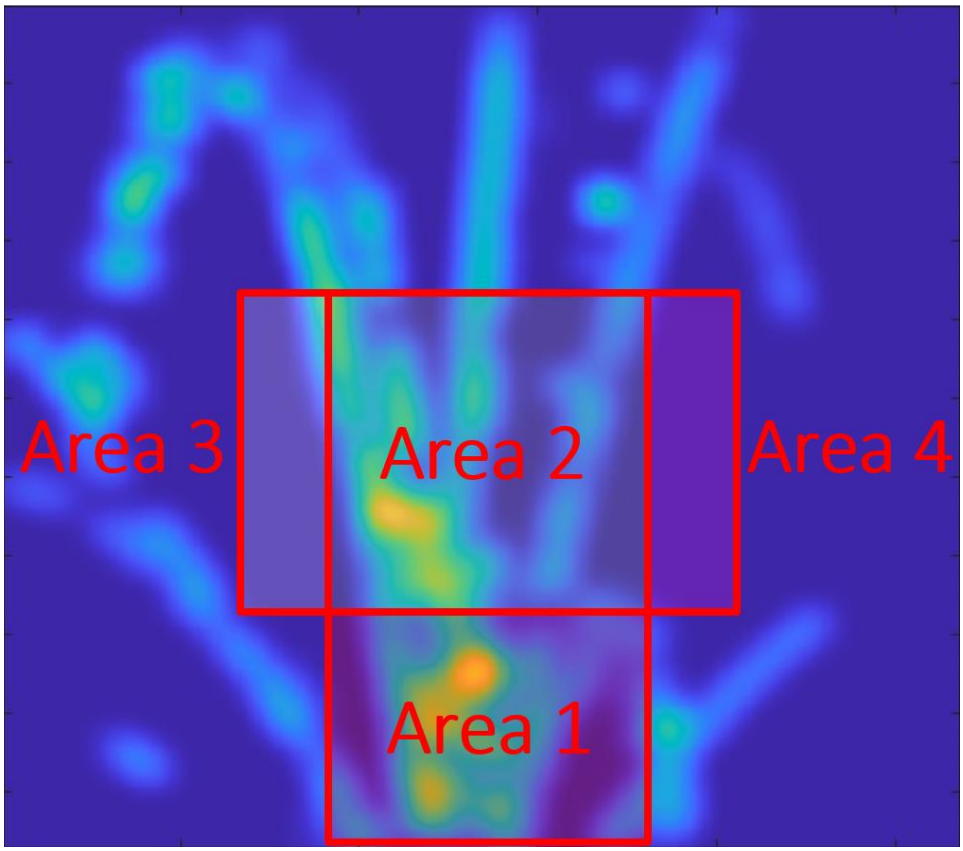

Fig. 26: Four regions considered.

The four areas had rectangular shape: the first region was placed quite above the nebulization device, the second was always in the centre of the image, in an upper position with respect to the first one, the third was on the left side, and the fourth and last one was on the right side. The rectangle defining the region 1 had coordinates [225 350 175 200], and after its definition, particles with x-coordinate involved between 225 and 400 and y-coordinate between 350 and 550. After selection of the desired particles, a new matrix, corresponding to the data in the investigated region was created, including only the rows of the initial matrix satisfying the previous condition. The same process has been performed for all the four regions: for the second the area was delimited by the rectangle [225 149 175 200], for the third it was [125 150 100 300], and the fourth was [401 150 50 300].

For each region it was represented the velocity distribution by plotting a histogram of the third column of the matrix, and by considering the values of velocity higher than 0,1 m/s, in order to remove the slower contributions that were considered outliers. For a statistical analysis some statistical indices have been computed, such as the median, the 25th percentile and the 75th percentile of each region. If Fig.27 an example of histogram for the velocity distribution is shown, related to the second region with the configuration of pressure equal to 2 bar and blowing time of 0,2 s.

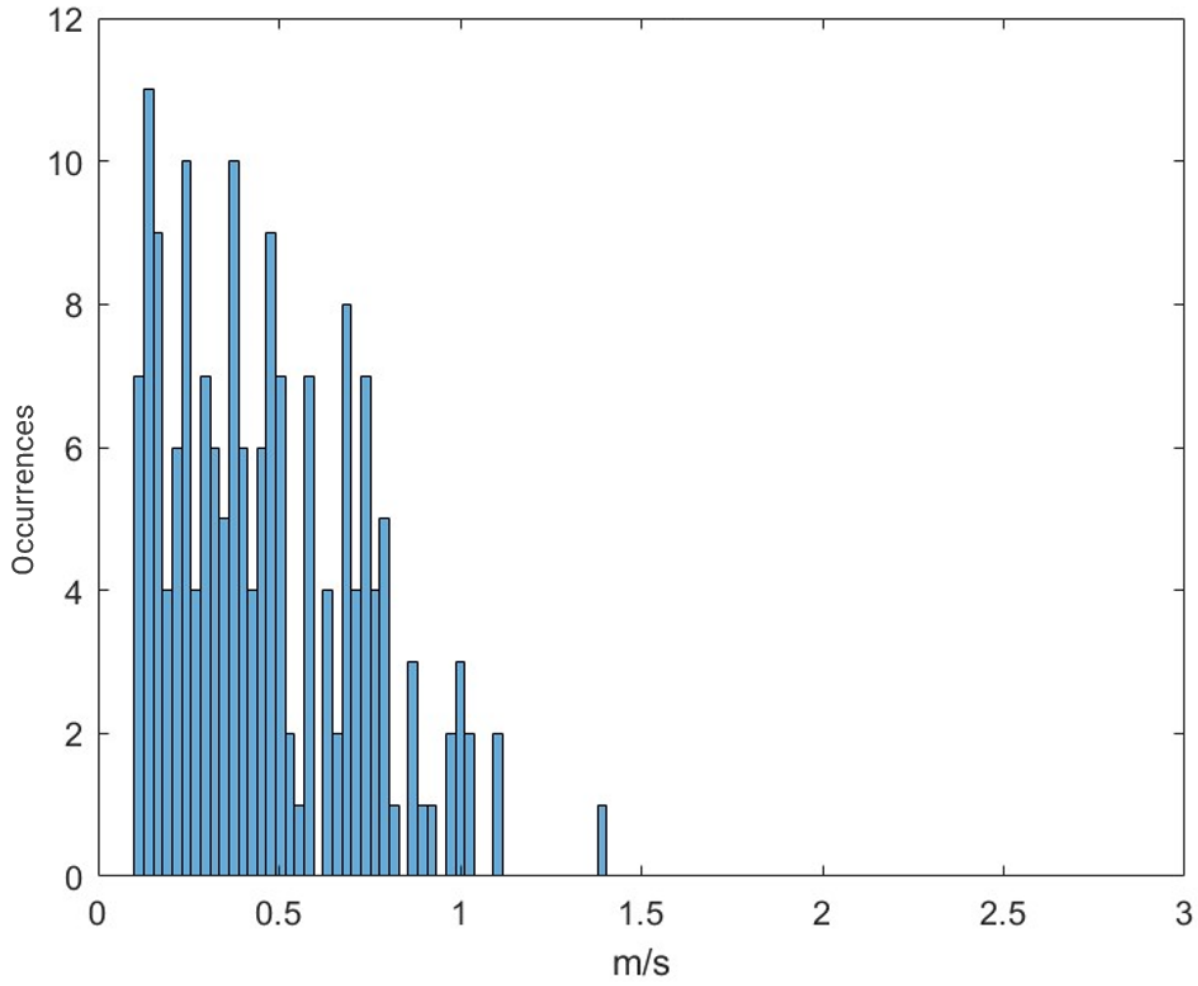

Fig. 27: Example of histogram representation of the velocity for each region.

For each combination of the parameters of pressure and blowing time, the histogram representation of the median values of each region was created, to evaluate the difference between velocities in the four areas.

The same type of statistical analysis has been performed to investigate the diameters of the particles. The fourth column of the matrix has been selected, since it was the one corresponding to the dimension of the particles, and it has been multiplied by a conversion factor, which performs the conversion from the pixel representation to the mm representation, since from the calibration grid shown in Fig.19 it results 5mm correspondence to 100 pixels.

Once the best configuration was found, more acquisitions have been performed, precisely 30 videos, to have a more complete representation of the nebulization and visualization of the velocity map.

Chapter 3: Results

A visual representation of the velocity distribution obtained for the three considered combinations of parameter is shown in Fig.28. Different values of velocity are associated to different colours in the colour scale.

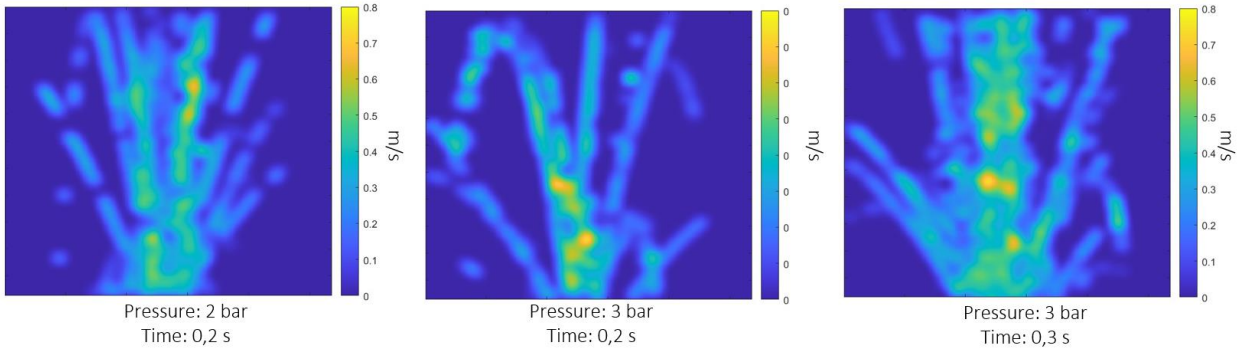

Fig.28: Velocity distribution of the surfactant in the three combinations of test parameters.

Results about the velocity and dimension distributions for each of the four considered areas are shown below.

REGION 1.

In Fig.29 there's the representations of the velocity distributions of surfactant in the first region. On the left side of the image, there's the configuration of pressure 2 bar and blowing time 0,2 s; in the centre of the image there's the configuration with 3 bar and 0,2 s; on the right side there's the velocity distribution associated with pressure of 3 bar and blowing time of 0,3 s. In Fig. 30 the dimension distribution of particles in area 1 is shown, for the three combinations of parameters.

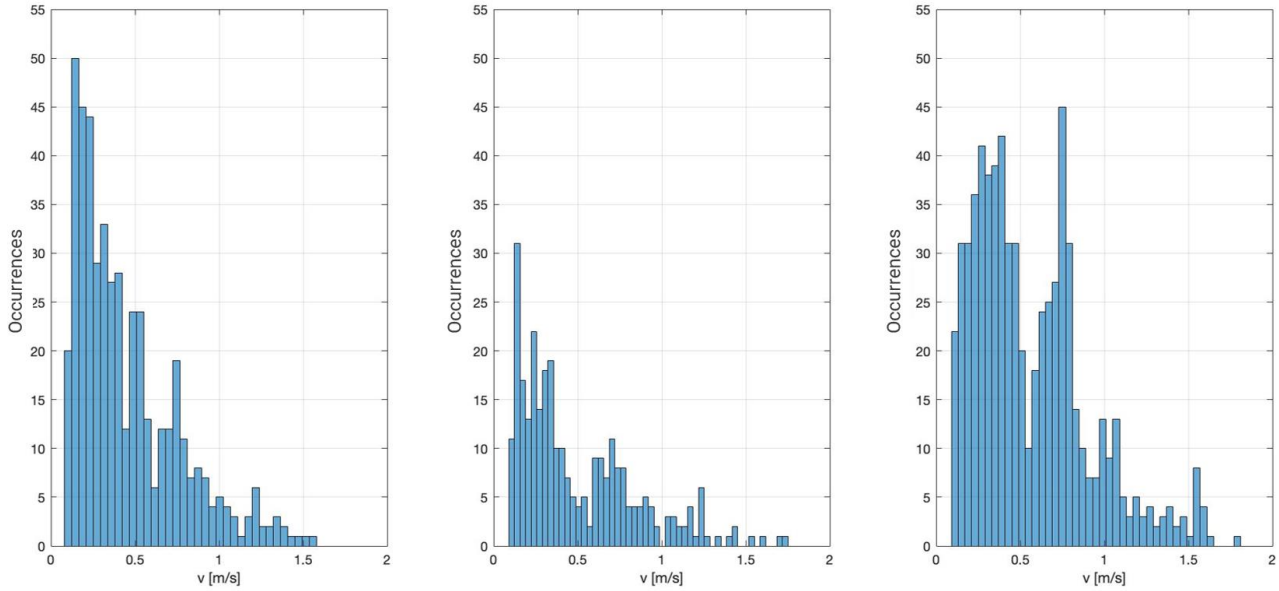

Fig. 29: Velocity distribution in region 1.

In Table 3, results about median,25th percentile and 75th percentile of velocity associated to area 1 are reported, for the three different configurations. In table 4 are reported the same statistical indices, but for the dimension distribution.

Velocity [m/s]	Pressure: 2 bar Time: 0,2 s	Pressure: 3 bar Time: 0,2 s	Pressure: 3 bar Time: 0,3 s
Median	0,36	0,36	0,47
25th percentile	0,21	0,23	0,29
75th percentile	0,63	0,72	0,76

Table 2: Median, 25th and 75th percentile of the velocity in region 1.

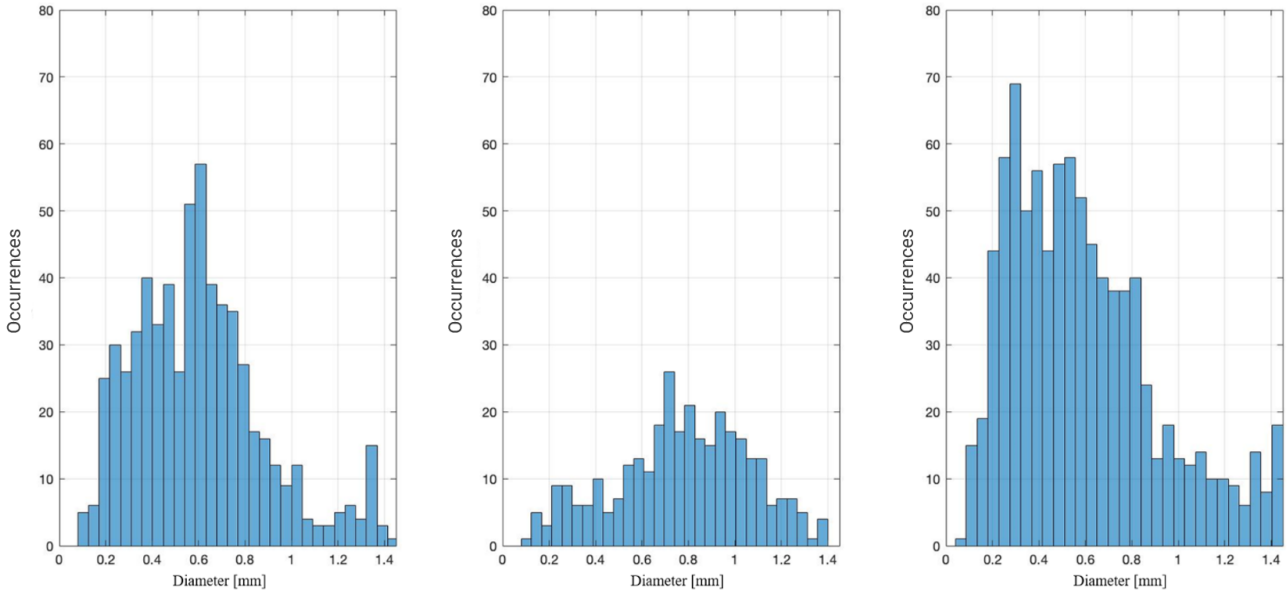

Fig. 30: Dimension distribution in region 1.

Diameter [mm]	Pressure: 2 bar Time: 0,2 s	Pressure: 3 bar Time: 0,2 s	Pressure: 3 bar Time: 0,3 s
Median	0,58	0,78	0,54
25th percentile	0,39	0,58	0,33
75th percentile	0,75	0,98	0,77

Table 3: Median, 25th and 75th percentile of the diameter in region 1.

REGION 2.

In Fig.31 and Fig.32, respectively, there's the representations of the velocity distributions and dimension distributions of particles in region 2, for all the three configurations.

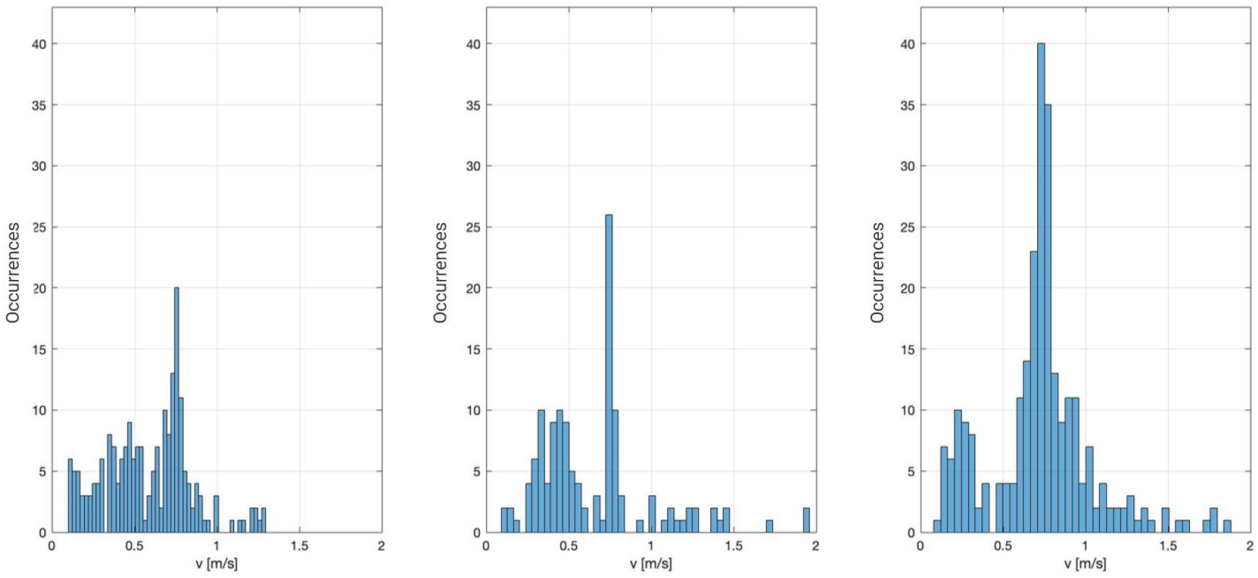

Fig. 31: Velocity distribution in the region 2.

In Table 5 the results about median,25th percentile and 75th percentile of velocity in region 2 are reported, for the three different configurations. In table 6 the same indices are displayed for the dimension distribution in the same region.

Velocity [m/s]	Pressure: 2 bar Time: 0,2 s	Pressure: 3 bar Time: 0,2 s	Pressure: 3 bar Time: 0,3 s
Median	0,61	0,58	0,74
25th percentile	0,38	0,40	0,60
75th percentile	0,75	0,76	0,84

Table 4: Median, 25th and 75th percentile of the velocity in the region 2.

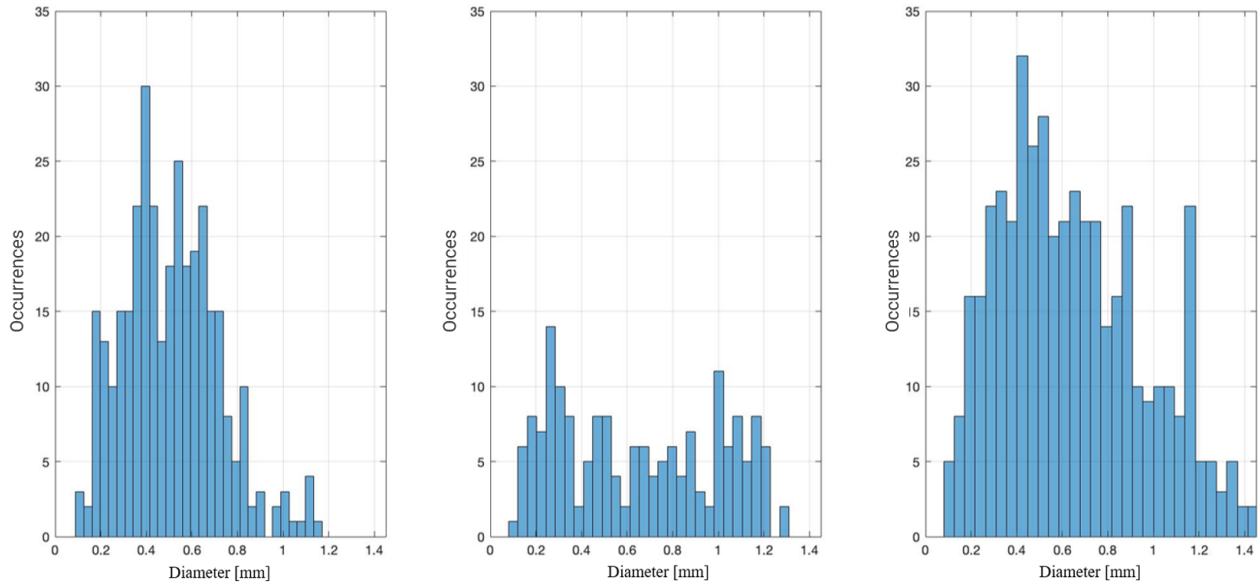

Fig. 32: Dimension distribution in region 2.

Diameter [mm]	Pressure: 2 bar Time: 0,2 s	Pressure: 3 bar Time: 0,2 s	Pressure: 3 bar Time: 0,3 s
Median	0,49	0,63	0,60
25th percentile	0,36	0,31	0,40
75th percentile	0,64	1	0,86

Table 5: Median, 25th and 75th percentile of the diameter in the region 2.

REGION 3.

In Fig.33 and Fig.34, respectively, there's the representations of the velocity distributions and dimension distributions of particles in region 3.

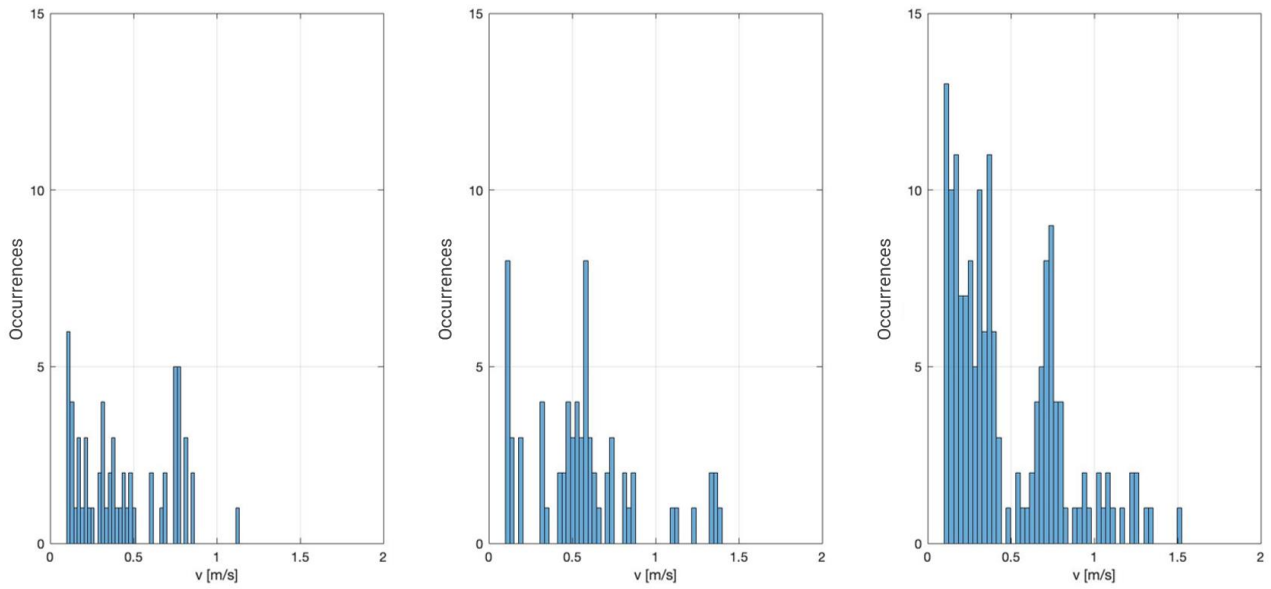

Fig. 33: Velocity distribution in the region 3.

In Table 7 and Table 8 there are the results about median,25th percentile and 75th percentile of velocity and dimension, respectively, in region 3, for all combinations of parameters.

Velocity [m/s]	Pressure: 2 bar Time: 0,2 s	Pressure: 3 bar Time: 0,2 s	Pressure: 3 bar Time: 0,3 s
Median	0,38	0,54	0,35
25th percentile	0,20	0,32	0,20
75th percentile	0,74	0,70	0,71

Table 6: Median, 25th and 75th percentile of the velocity in the region 3.

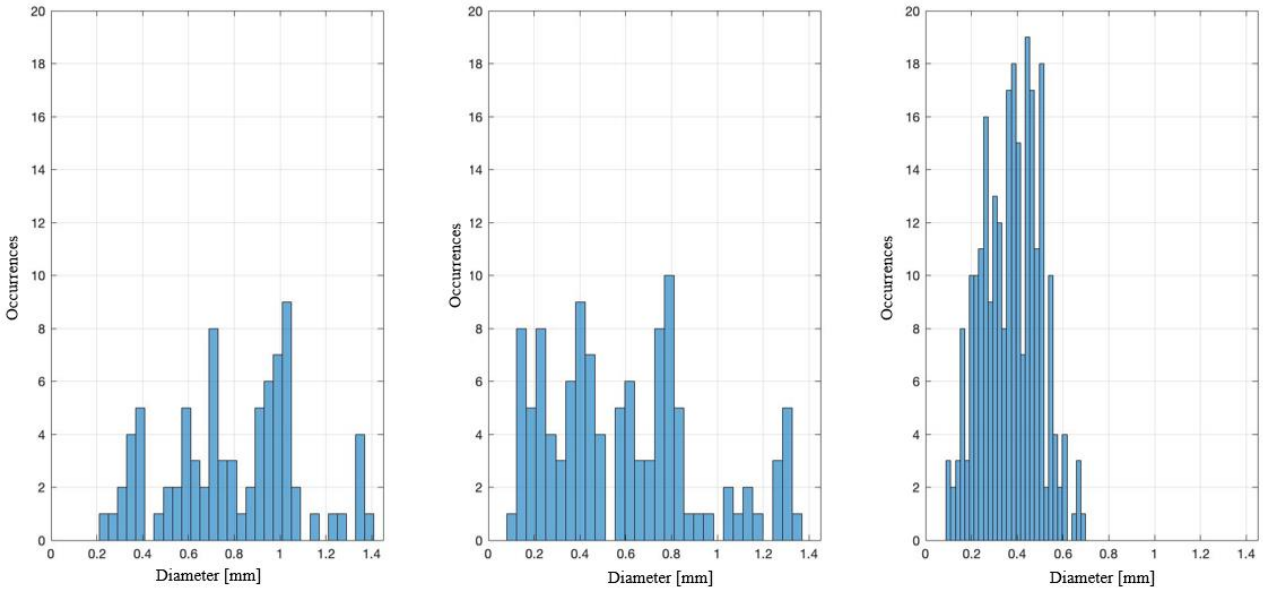

Fig. 34: Dimension distribution in the region 3.

Diameter [mm]	Pressure: 2 bar Time: 0,2 s	Pressure: 3 bar Time: 0,2 s	Pressure: 3 bar Time: 0,3 s
Median	0,80	0,56	0,37
25th percentile	0,59	0,32	0,26
75th percentile	1.01	0,79	0,46

Table 7: Median, 25th and 75th percentile of the diameter in the region 3.

REGION 4.

In Fig.35 and Fig.36, respectively, velocity and dimension distributions of particles in region 4 are respectively shown. In Table 9 and Table 10 there are the results about median,25th percentile and 75th percentile of velocity and dimension in region 4, for all combinations of parameters.

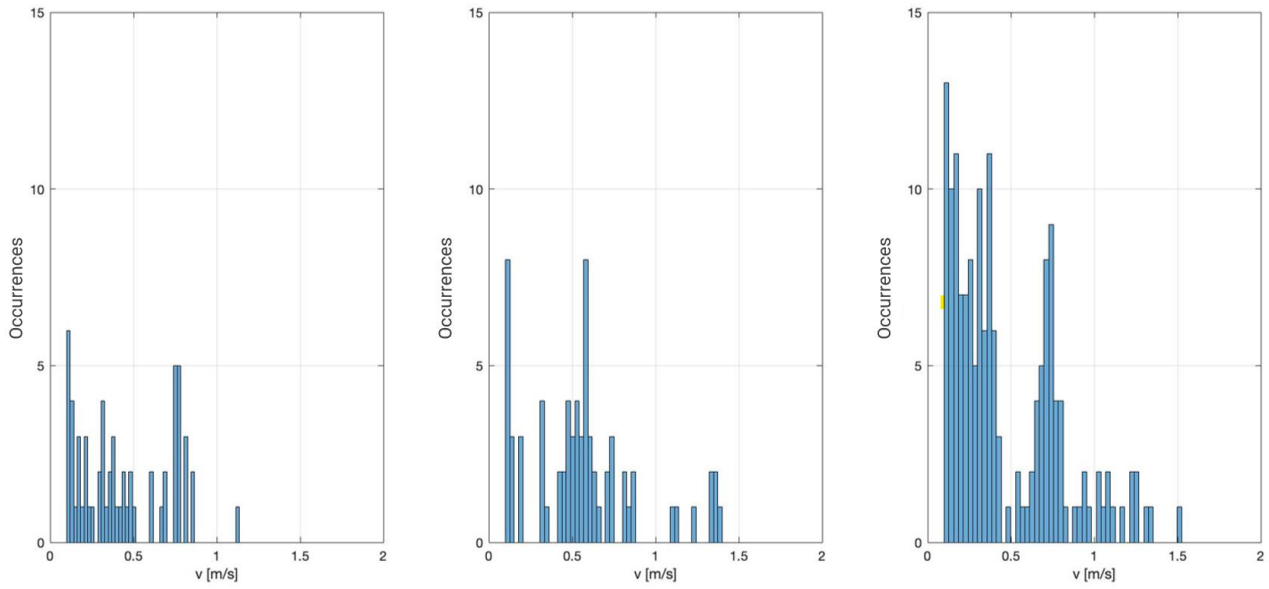

Fig. 35: Velocity distribution in the region 4.

Velocity [m/s]	Pressure: 2 bar Time: 0,2 s	Pressure: 3 bar Time: 0,2 s	Pressure: 3 bar Time: 0,3 s
Median	0,31	0,38	0,26
25th percentile	0,14	0,28	0,18
75th percentile	0,43	0,46	0,70

Table 8: Median, 25th and 75th percentile of the velocity in the region 4.

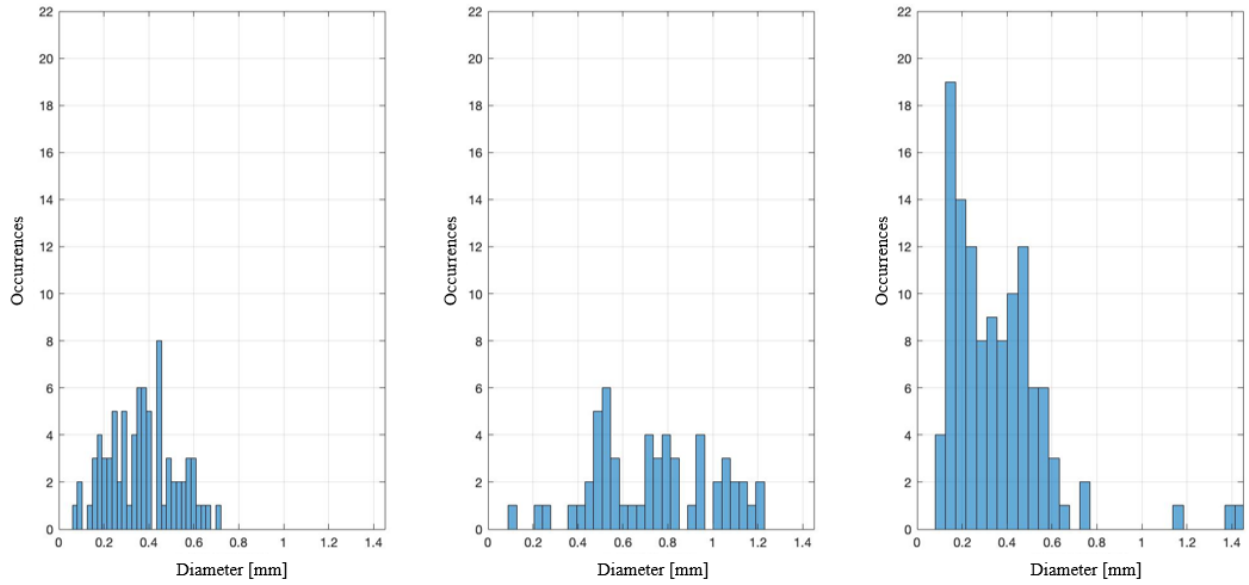

Fig. 36: Dimension distribution in the region 4.

Diameter [mm]	Pressure: 2 bar Time: 0,2 s	Pressure: 3 bar Time: 0,2 s	Pressure: 3 bar Time: 0,3 s
Median	0,36	0,71	0,31
25th percentile	0,24	0,51	0,20
75th percentile	0,46	0,95	0,47

Table 9: Median, 25th and 75th percentile of the diameter in the region 4.

A comparison of the median values of velocity and dimensions of the particles was performed, to characterize the best configuration and the region were there's higher efficiency of the nebulization. Results obtained are shown in Fig.37 and Fig.38, where the histogram of the median values for each configuration are compared, for all the four regions.

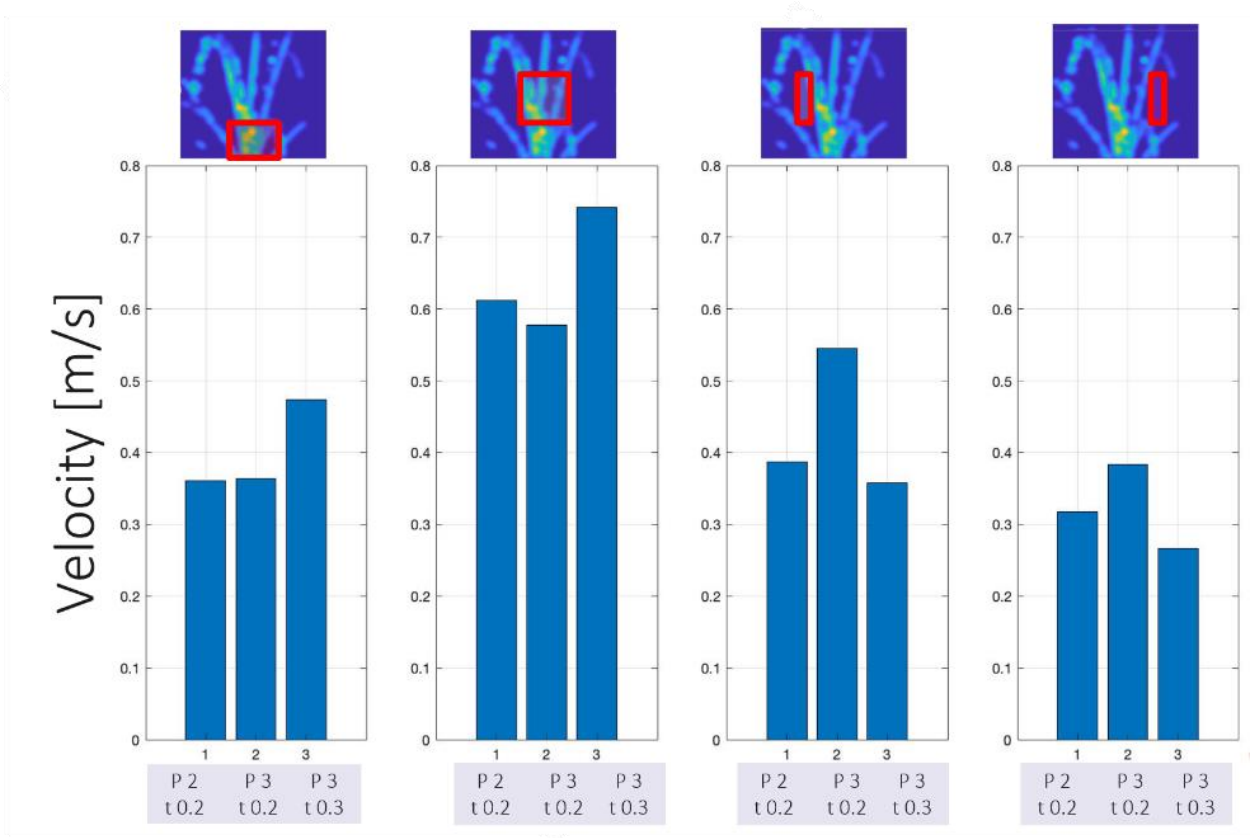

Fig. 37: Comparison between velocities values with all configurations in the four areas.

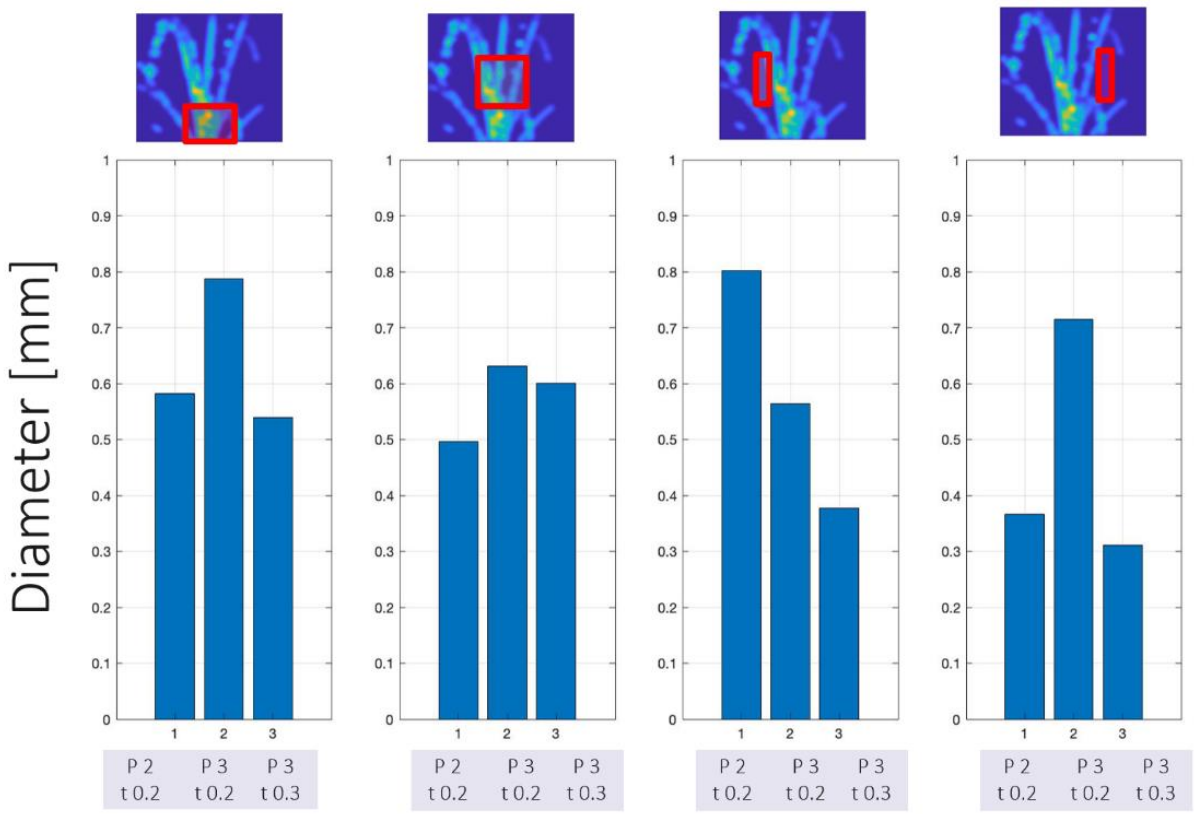

Fig. 38: Comparison between diameter values with all configurations in the four areas.

The successive part of the analysis consisted of finding the best configuration between the investigated one: it resulted to be the one with pressure of 3 bar and blowing time of 0,3 s. The chromatic representation result of the velocity in this configuration, with more acquisitions considered as previously explained, is shown below.

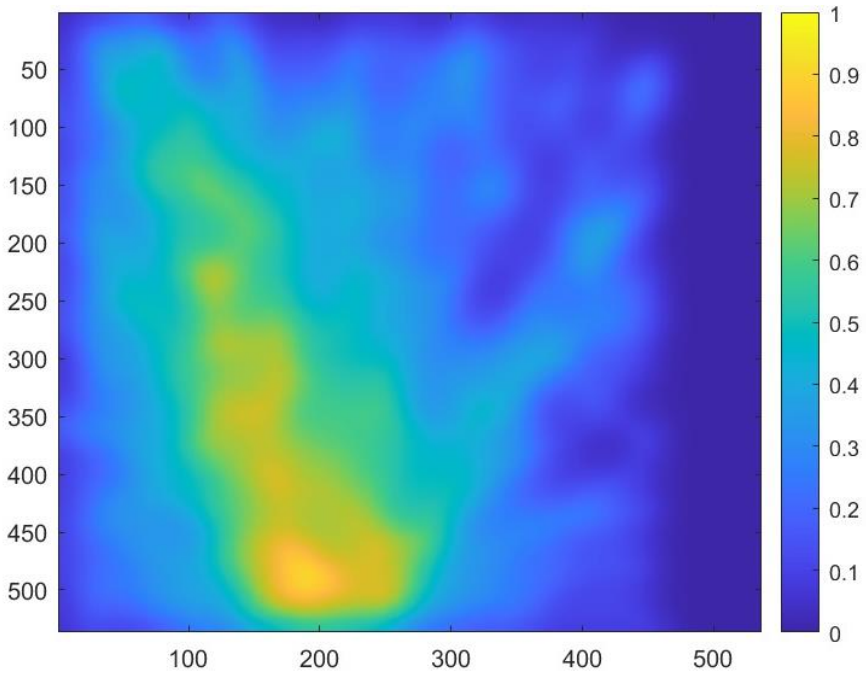

Fig. 39: Velocity distribution of the best configuration, with pressure 3 bar and blowing time 0,3 s.

For the selected configuration, median values of velocity and dimension were computed, to understand the differences between the four regions. Results about the velocity values are shown in Fig. 40 and Table 11, results about dimensions are shown in Fig.41 and Table 12.

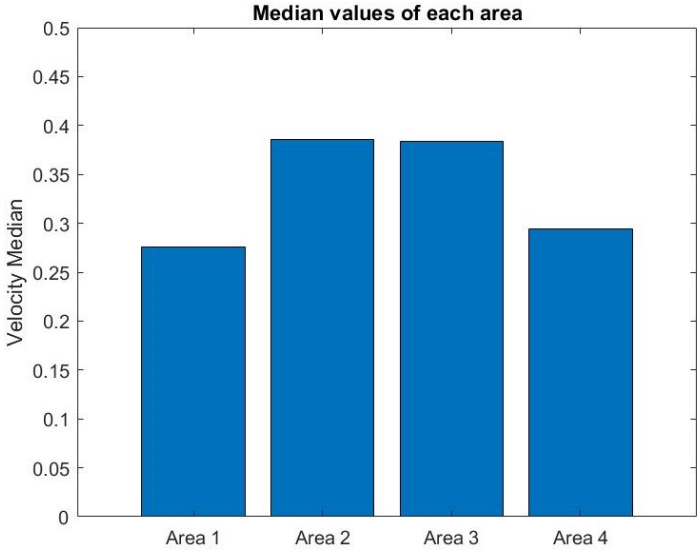

Fig. 40: Median of the velocity values in the four regions, for the configuration with 3 bar and 0,3 s.

Velocity [m/s]	Area 1	Area 2	Area 3	Area 4
Median	0,28	0,39	0,38	0,29
25th percentile	0,19	0,21	0,23	0,23
75th percentile	0,43	0,67	0,65	0,45

Table 10: Median, 25th and 75th percentile of the velocity in the four areas, for the configuration with pressure 3 bar and blowing time 0,3 s.

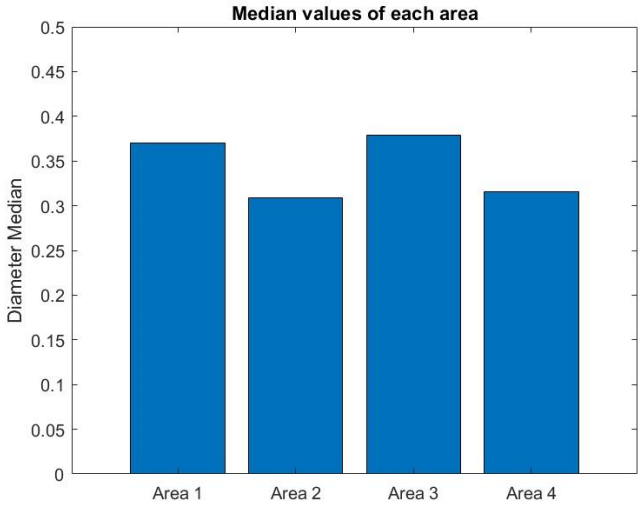

Fig. 41: Median of the diameter values in the four regions, for the configuration with 3 bar and 0,3 s.

Diameter [mm]	Area 1	Area 2	Area 3	Area 4
Median	0,37	0,31	0,38	0,31
25th percentile	0,26	0,22	0,27	0,22
75th percentile	0,54	0,43	0,54	0,43

Table 11: Median, 25th and 75th percentile of the diameter in the four areas, for the configuration with pressure 3 bar and blowing time 0,3 s.

In the following figure it will be displayed the comparison between the different particle behaviours in more planes, at different distances from the nebulization source. Each plane was considered as a separate slice, and it was illuminated with a laser, so to exclude all the contributions out of the desired slice.

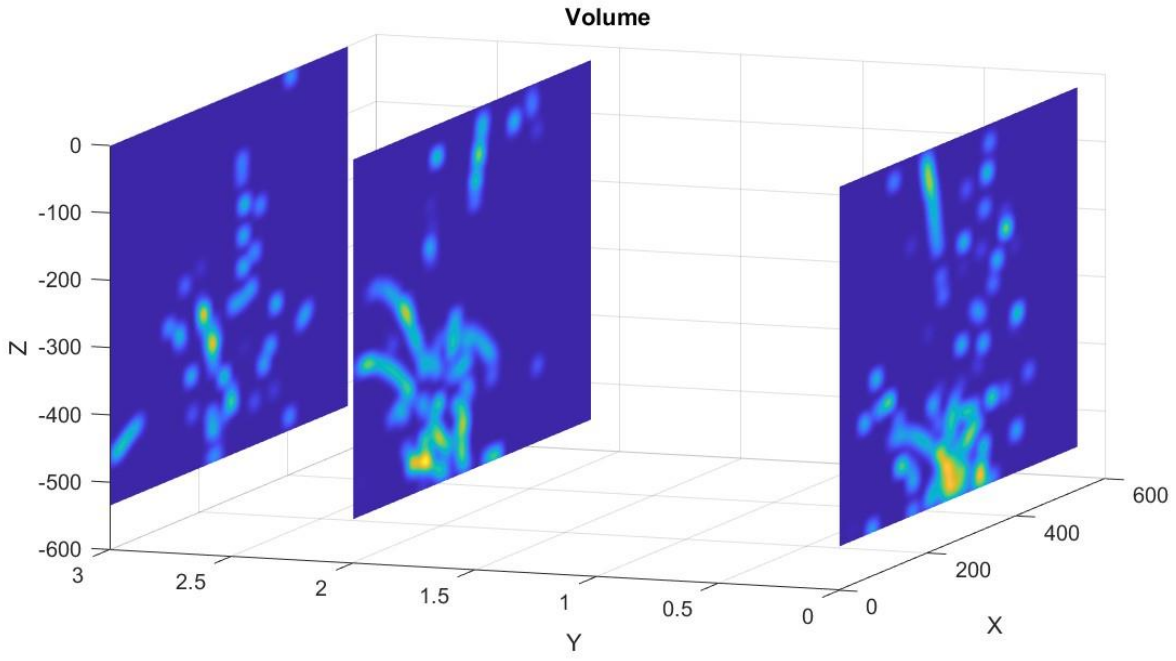

Fig. 42: Velocity distribution in the three planes, with position shown in Y axis.

Chapter 4: Discussion and Conclusion

4.1. *Discussion and conclusion*

Fig.28 represents the distribution of velocities in the different configurations. Considering for all of them a minimum limit of 0 m/s and a maximum of 0.8 m/s, it can be seen that for 2 bar and 0.2 s, there are on average lower velocities than for the rest, with 3 bar and 0.2 s higher velocities are reached, which however do not characterize a large number of particles, while with the last configuration, there are more fast particles, with a jet concentrated mainly in the most central area of the atomization.

Velocity and dimension distributions in the three configurations for the first region (Fig.29 and Fig. 30) show that for the configuration with 3 bar and 0.3 s the particles reach higher velocities, with a median value of 0.47 as shown in Table 3, while for the other configurations most of the particles are slower. At the same time, the particles in the configuration previously considered turn out to have a smaller diameter than in other configurations (Table 4).

The results inherent in the second region (Fig.31 and Fig.32) show higher velocities for the same configuration as before, with an even higher average value, as Table 5 shows a median velocity value of 0.74 m/s, while the other configurations there are fewer particles and also slower. In this case, it can be seen that the smallest particles are associated with the 2 bar and 0.2 s configuration, but this is also due to fewer particles reaching the area concerned. In fact, of the two configurations with higher velocities, the smallest particles are those generated by the combination of 3 bar and 0.3 s, thus the fastest (Table 6).

Fig.33 and Fig.34 show the velocities and diameters in region 3, which is one of the two side regions. In this case, the highest velocity is associated with 3 bar and 0.2 s; therefore, there is no agreement with the results of the two previous regions since the configuration considered

above shows the lowest velocities (Table 7). This result may be because in this configuration, as seen above, the particles tend to be pushed more in the direction above the atomizer, so fewer particles reach the side zones and maybe the ones that fall back are attracted by gravity. This could be confirmed by the fact that in 3 bar, 0.3 s configuration, there are also the smallest particles, as shown in Table 8, and that they are therefore accelerated more in the central zones, and laterally they tend to slow down.

In the area 4 (Fig.35 and Fig.36) lower velocities appear, with behaviour very similar to that in area 3, both being two lateral regions.

A clearer comparison of the median velocity values in the three configurations for each region is shown in Fig.37, from which it can be deduced that in the two side areas, there are generally lower velocities for all configurations, while the highest velocities occur for regions 1 and 2. Precisely, faster particles are identified for all combinations in Region 2, with the configuration at 3 bar and 0.3 s having the highest value of all. In Fig.38 there is a comparison of the diameter values in all configurations for each region. It can be deduced that, on average, the smallest particles are those associated with the 3 bar and 0.3 s configuration, which are generally the fastest.

After analysing the behaviour of the particles for the various configurations and regions, it was investigated the best configuration through a larger number of acquisitions. A colour map showing the velocity distribution under these conditions is shown in Fig.39, where a higher particle velocity can be observed in the two central zones, as also expected from previous results. A histogram of the velocity values in the 4 areas is depicted and shows greater values achieved in region 2, i.e., the central region, higher up the nebulizer (Fig. 40). One consequence is that these fast particles are associated with a smaller diameter than the other areas, and this hypothesis is confirmed in Fig.41.

The volumetric velocity distribution, so the difference in the velocity values in the three planes at different distances from the nebulizer, shows that the closer the plane is to the nebulizer, the more velocities with higher values are focused closer to the nebulizer. By getting further from the nebulizer, the fastest particles are further from the nebulizer, because of the development of the nebulization. From Fig.37, it can be deduced that the highest velocities are reached for the configuration pressure 3 bar and blowing time 0,3 s in the central regions of the image, so 1 and 2, and with pressure 3 bar and blowing time 0,2 s for the side regions, so 3 and 4. So a longer blowing time is necessary to provide further a nebulization of the surfactant particles in the central area, closest to the nebulization device. By analysing the Fig.38 is also possible to see how diameters of particles vary with the configurations, and it can be seen that smallest particles are associated with pressure 3 bar and blowing time 0,3 s combination of parameters. This leads to the conclusion that the best configuration is the one with pressure of 3 bar and blowing time of 0,3 s, since to this correspond higher velocities and smaller particles. From the deeper analysis performed on this configuration of parameters, it has been deduced that the main velocity is reached in area 2 and area 3, as it can be observed in Fig.40. The smallest particles have been detected inside the second region, so this can lead to the conclusion that the region in which the nebulization is more efficient is the second one. The investigation of the nebulized jet slice by slice allowed to understand how the velocity changes with the distance from the nebulization source: the plane corresponding to the position of the source showed highest velocities quite closer to the nebulizer, while the more the slice gets further from the source, the more highest velocities are far from the source. This could be due to the acceleration felt by the particles because of the pressure during the ejection and because of the gravity during the descending motion of the particles.

The representation in Fig.39 shows that the highest velocities are in correspondence of the nebulizer, but there's then a developing of the highest values in a decentralized position: this could be associated with the asymmetry in the structure of the nebulization device itself.

To conclude, it can be said that based on the results obtained, the device is not yet efficient for use in endotracheal nebulisation, as the particles it produces are not fast enough or even small enough to fulfil its purpose. In fact, it is necessary for the particles to be much smaller than what was found in this study (Fig.9): it is necessary to have particles with a diameter in the range 1-5 μm to be able to reach the lower airways and thus the alveoli [31, 32], since larger particles (>10 μm) usually deposit in the upper airways and particles with diameter of 5-10 μm can reach at maximum large bronchi [32].

4.2. *Suggestion for future studies*

Further studies are needed to improve the device. Some possible ideas for testing will be liste d below.

1) Moving the surfactant outlet more to the centre to avoid asymmetry.

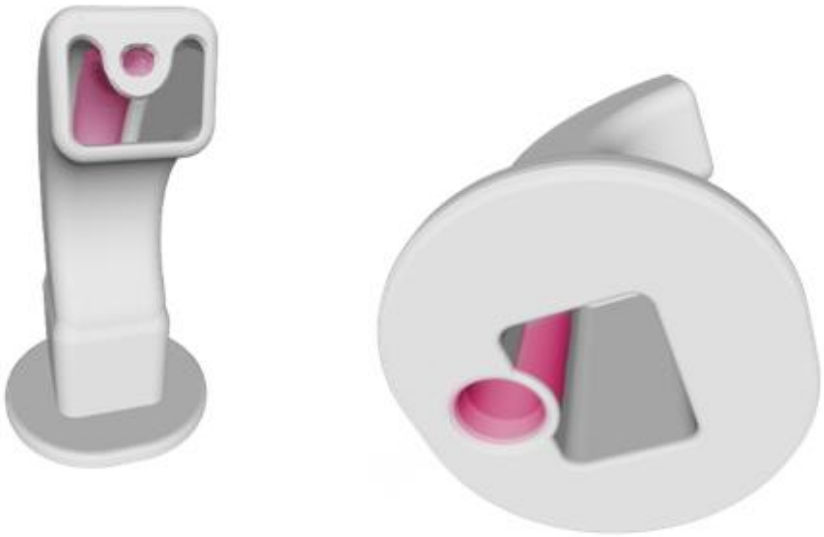

Fig. 43: Nebulizer with evidenced surfactant outlet.

The space in which the coaxial cable must be inserted could be displaced in a more centred position with respect to the one where it is placed, shown in picture. In this way the asymmetry of the velocity could be limited.

2) Reversing the coaxial cables of the connector to see if a better result is guaranteed.

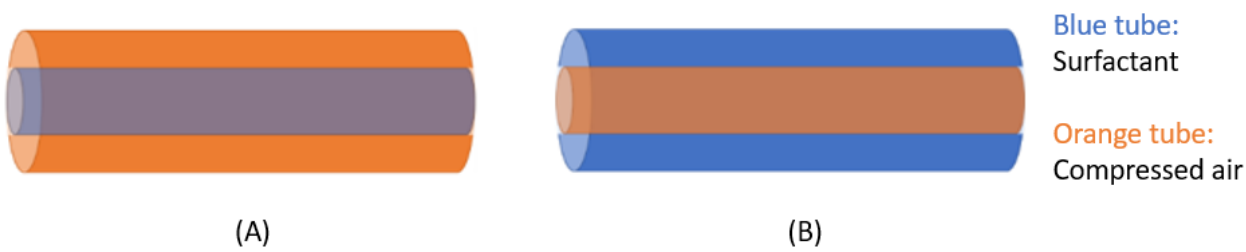

Fig. 44: Inversion of tubes in the coaxial cable.

Inside the outer tube there is the compressed air, inner tube contains the surfactant. The actual configuration is the one where the surfactant tube is inside the compressed air tube, as shown in (A) in Fig.44. An idea to improve the quality of the nebulization is to pass from the condition A to the condition B, so to invert the external and internal tubes.

3) Intervene on the connector by increasing the cable lumen with air to prevent the output pressure from being dampened, in particular in the point where the tubes are curved. A solution could be the increase of the compressed air tube diameter.
4) Secure the internal catheter carrying the surfactant since it tends to move and change the properties of the jet. The inner tube carrying the surfactant is not fixed inside the outer tube, so during the action it could move and slide up and down inside the bigger tube. This could lead to malfunctioning of the system, so a possible solution could be the stopping of the inner catheter by adding a stopper.

Figure index

Fig.1: Respiratory system 4

Fig. 2: Representation of pulmonary alveoli 5

Fig. 3: Representation of lungs with visceral pleura and parietal pleura 7

Fig. 4: Surfactant composition. 11

Fig. 5: Comparison between healthy alveoli and collapsed alveoli. 14

Fig. 6: Endotracheal system for surfactant delivery 17

Fig. 7: Representation of a pneumatic nebulizer 20

Fig. 8: Representation of an ultrasonic nebulizer 21

Fig. 9: Difference in particles dimension along the airways 23

Fig. 10: Measurement setup 25

Fig. 11: Scheme of the measurement setup 25

Fig. 12: Electro-pneumatic valve 27

Fig. 13: Syringe placed on the guide and actuator 28

Fig. 14: User interface 28

Fig. 15: T-shape modified connector. 29

Fig. 16: Device for the creation of the coaxial catheter. 29

Fig. 17: Nebulizer 30

Fig. 18: Model of the nebulizer 31

Fig. 19: Representation of the conversion grid. 36

Fig. 20: Block scheme of the steps of analysis 39

Fig. 21: Representation of acquired frame. 39

Fig. 22: Cropped frame 40

Fig. 23: Representation of the tracked velocity in two consecutive frames 42

Fig. 24: Example of the chromatic representation of the nebulization, for the configuration with pressure of 3 bar and blowing time of 0,3 s. 45

Fig. 25: Chromatic Representation of the different configurations of Pressure and Blowing Time 75

Fig. 26: Four regions considered. 47

Fig. 27: Example of histogram representation of the velocity for each region 48

Fig. 28: Velocity distribution of the surfactant in the three combinations of test parameters 50

Fig. 29: Velocity distribution in region 1. 51

Fig. 30: Dimension distribution in region 1 52

Fig. 31: Velocity distribution in the region 2. 53

Fig. 32: Dimension distribution in region 2. 54

Fig. 33: Velocity distribution in the region 3 55

Fig. 34: Dimension distribution in the region 3. 56

Fig. 35: Velocity distribution in the region 4 57

Fig. 36: Dimension distribution in the region 4. 58

Fig. 37: Comparison between velocities values with all configurations in the four areas 59

Fig. 38: Comparison between diameter values with all configurations in the four areas 60

Fig. 39: Velocity distribution of the best configuration, with pressure 3 bar and blowing time 0,3 s. 75

Fig. 40: Median of the velocity values in the four regions, for the configuration with 3 bar and 0,3 s. 61

Fig. 41: Median of the diameter values in the four regions, for the configuration with 3 bar and 0,3 s. 62

Fig. 42: Velocity distribution in the three planes, with position shown in Y axis 64

Fig. 43: Nebulizer with evidenced surfactant outlet 69

Fig. 44: Inversion of tubes in the coaxial cable 70

Table index

Table 1: Measuring protocol for water analysis. 33

Table 2: Measuring protocol for surfactant analysis 34

Table 3: Median, 25th and 75th percentile of the velocity in region 1 51

Table 4: Median, 25th and 75th percentile of the diameter in region 1 52

Table 5: Median, 25th and 75th percentile of the velocity in the region 2 53

Table 6: Median, 25th and 75th percentile of the diameter in the region 2 54

Table 7: Median, 25th and 75th percentile of the velocity in the region 3 55

Table 8: Median, 25th and 75th percentile of the diameter in the region 3 56

Table 9: Median, 25th and 75th percentile of the velocity in the region 4. 57

Table 10: Median, 25th and 75th percentile of the diameter in the region 4 58

Table 11: Median, 25th and 75th percentile of the velocity in the four areas, for the configuration with pressure 3 bar and blowing time 0,3 s 62

Table 12: Median, 25th and 75th percentile of the diameter in the four areas, for the configuration with pressure 3 bar and blowing time 0,3 s. 63

Bibliography

[1] Fisiologia – 9788895033501, di Scotto P. (cur.) Mondola P. (cur.) edito da Poletto Editore, 2012

[2] Parra E, Pérez-Gil J. Composition, structure and mechanical properties define performance of pulmonary surfactant membranes and films. Chem Phys Lipids. 2015 Jan;185:153-75. doi: 10.1016/j.chemphyslip.2014.09.002. Epub 2014 Sep 28. PMID: 25260665.

[3] https://www.gradenigo.it/enciclopedia/anatomia/apparato-respiratorio/

[4] https://pspediatrico.policlinicogemelli.it/wp-content/uploads/2019/01/Per-gli-infermieri-Vie-respiratorie.pdf

[5] https://www.ospedalebambinogesu.it/anatomia-dell-apparato-respiratorio-nei-bambini-90010/

[6] Goerke J. Pulmonary surfactant: functions and molecular composition. Biochim Biophys Acta. 1998 Nov 19;1408(2-3):79-89. doi: 10.1016/s0925-4439(98)00060-x. PMID: 9813251.

[7] Hallman M. The surfactant system protects both fetus and newborn. Neonatology. 2013;103(4):320-6. doi: 10.1159/000349994. Epub 2013 May 31. PMID: 23736009.

[8] Rebello CM, Jobe AH, Eisele JW, Ikegami M. Alveolar and tissue surfactant pool sizes in humans. Am J Respir Crit Care Med. 1996 Sep;154(3 Pt 1):625-8. doi: 10.1164/ajrccm.154.3.8810596. PMID: 8810596.

[9] Andreassen S, Steimle KL, Mogensen ML, Bernardino de la Serna J, Rees S, Karbing DS. The effect of tissue elastic properties and surfactant on alveolar stability. J Appl Physiol (1985). 2010 Nov;109(5):1369-77. doi: 10.1152/japplphysiol.00844.2009. Epub 2010 Aug 19. PMID: 20724566; PMCID: PMC2980374.

[10] Liu M, Wang L, Li E, Enhorning G. Pulmonary surfactant given prophylactically alleviates an asthma attack in guinea-pigs. Clin Exp Allergy. 1996 Mar;26(3):270-5. PMID: 8729663.

[11] Im Hof V, Gehr P, Gerber V, Lee MM, Schürch S. In vivo determination of surface tension in the horse trachea and in vitro model studies. Respir Physiol. 1997 Jul;109(1):81-93. doi: 10.1016/s0034-5687(97)84032-7. PMID: 9271810.

[12] De Sanctis GT, Tomkiewicz RP, Rubin BK, Schürch S, King M. Exogenous surfactant enhances mucociliary clearance in the anaesthetized dog. Eur Respir J. 1994 Sep;7(9):1616-21. doi: 10.1183/09031936.94.07091616. PMID: 7995390.

[13] Schürch S, Goerke J, Clements JA. Direct determination of surface tension in the lung. Proc Natl Acad Sci U S A. 1976 Dec;73(12):4698-702. doi: 10.1073/pnas.73.12.4698. PMID: 1070020; PMCID: PMC431602.

[14] Lee MM, Schürch S, Roth SH, Jiang X, Cheng S, Bjarnason S, Green FH. Effects of acid aerosol exposure on the surface properties of airway mucus. Exp Lung Res. 1995 Nov-Dec;21(6):835-51. doi: 10.3109/01902149509031766. PMID: 8591789.

[15] Sardesai S, Biniwale M, Wertheimer F, Garingo A, Ramanathan R. Evolution of surfactant therapy for respiratory distress syndrome: past, present, and future. Pediatr Res. 2017 Jan;81(1-2):240-248. doi: 10.1038/pr.2016.203. Epub 2016 Oct 5. PMID: 27706130

[16] Devi U, Pandita A. Surfactant delivery via thin catheters: Methods, limitations, and outcomes. Pediatr Pulmonol. 2021 Oct;56(10):3126-3141. doi: 10.1002/ppul.25599. Epub 2021 Aug 11. PMID: 34379878.

[17] De Luca D, Autilio C. Strategies to protect surfactant and enhance its activity. Biomed J. 2021 Dec;44(6):654-662. doi: 10.1016/j.bj.2021.07.011. Epub 2021 Aug 5. PMID: 34365021; PMCID: PMC8847817.

[18] McPherson C, Wambach JA. Prevention and Treatment of Respiratory Distress Syndrome in Preterm Neonates. Neonatal Netw. 2018 May 1;37(3):169-177. doi: 10.1891/0730-0832.37.3.169. PMID: 29789058.

[19] Warren JB, Anderson JM. Core concepts: respiratory distress sydrome. NeoReviews. 2009;10:e351-e361.

[20] Hallman M, Glumoff V, Rämet M. Surfactant in respiratory distress syndrome and lung injury. Comp Biochem Physiol A Mol Integr Physiol. 2001 May;129(1):287-94. doi: 10.1016/s1095-6433(01)00324-5. PMID: 11369552.

[21] Lankenau HM. A genetic and statistical study of the respiratory distress syndrome. Eur J Pediatr. 1976 Oct 1;123(3):167-77. doi: 10.1007/BF00452094. PMID: 976282.

[22] Klein JM, Nielsen HC. Androgen regulation of epidermal growth factor receptor binding activity during fetal rabbit lung development. J Clin Invest. 1993 Feb;91(2):425-31. doi: 10.1172/JCI116218. PMID: 8432851; PMCID: PMC287946.

[23] Gupta S, Donn SM. Continuous Positive Airway Pressure: To Bubble or Not to Bubble? Clin Perinatol. 2016 Dec;43(4):647-659. doi: 10.1016/j.clp.2016.07.003. PMID: 27837750.

[24] Samir Gupta, Steven M. Donn, Continuous positive airway pressure: Physiology and comparison of devices, Seminars in Fetal and Neonatal Medicine, Volume 21, Issue 3, 2016, Pages 204-211, ISSN 1744-165X, https://doi.org/10.1016/j.siny.2016.02.009.

[25] Gupta S, Donn SM: Continuous positive airway pressure: To bubble or not to bubble? Clin Perinatol 43(4):647–659, 2016. doi: 10.1016/j.clp.2016.07.003

[26] Mehler K, Broer A, Roll C, Göpel W, Wieg C, Jahn P, Teig N, Höhn T, Welzing L, Vochem M, Hoppenz M, Bührer C, Franklin J, Roth B, Herting E, Kribs A. Developmental outcome of extremely preterm infants is improved after less invasive surfactant application: Developmental outcome after LISA. Acta Paediatr. 2021 Mar;110(3):818-825. doi: 10.1111/apa.15565. Epub 2020 Sep 25. PMID: 32892376.

[27] Härtel C, Paul P, Hanke K, Humberg A, Kribs A, Mehler K, Vochem M, Wieg C, Roll C, Herting E, Göpel W. Less invasive surfactant administration and complications of preterm birth. Sci Rep. 2018 May 29;8(1):8333. doi: 10.1038/s41598-018-26437-x. PMID: 29844331; PMCID: PMC5974027

[28] G. Bartolozzi. Il surfattante nella difficoltà respiratoria del pretermine e del nato a termine. Medico e Bambino pagine elettroniche 2008;11(4) https://www.medicoebambino.com/?id=AP0804_10.html

[29] Herting, Egbert, Christoph Härtel, and Wolfgang Göpel. "Less invasive surfactant administration (LISA): chances and limitations." Archives of Disease in Childhood-Fetal and Neonatal Edition 104.6 (2019): F655-F659.

[30] Efficacia della metodica insure durante la CPAP in neonati prematuri affetti da syndrome da distress respiratorio. Leone F., Trevisanuto D., Cavallin F., Parotto M., Zanardo V.

[31] O'Callaghan C, Barry PW. The science of nebulised drug delivery. Thorax. 1997 Apr;52 Suppl 2(Suppl 2):S31-44. doi: 10.1136/thx.52.2008.s31. PMID: 9155849; PMCID: PMC1765865.

[32] B. D. S. S. e. a. Gardenhire DS, A Guide to Aerosol Delivery Devices for Respiratory Therapists, American Association for Respiratory Care, 2017.